INSTITUTE OF PHYSICS PUBLISHING REPORTS ON PROGRESS IN PHYSICS

Rep. Prog. Phys. **64** (2001) 1427–1472 PII: S0034-4885(01)14006-6

Models of permeation in ion channels

Serdar Kuyucak[1], **Olaf Sparre Andersen**[2] **and Shin-Ho Chung**[1]

[1] Department of Theoretical Physics, Research School of Physical Sciences, Australian National University, Canberra, ACT 0200, Australia
[2] Department of Physiology and Biophysics, Weill Medical College of Cornell University, 1300 York Avenue, New York, NY 10021-4896, USA

E-mail: serdar.kuyucak@anu.edu.au, sparre@pop.med.cornell.edu and shin-ho.chung@anu.edu.au

Received 25 July 2001, in final form 24 September 2001
Published 25 October 2001
Online at stacks.iop.org/RoPP/64/1427

Abstract

Ion channels are formed by specific proteins embedded in the cell membrane and provide pathways for fast and controlled flow of selected ions down their electrochemical gradient. This activity generates action potentials in nerves, muscles and other excitable cells, and forms the basis of all movement, sensation and thought processes in living beings. While the functional properties of ion channels are well known from physiological studies, lack of structural knowledge has hindered development of realistic theoretical models necessary for understanding and interpretation of these properties. Recent determination of the molecular structures of potassium and mechanosensitive channels from x-ray crystallography has finally broken this impasse, heralding a new age in ion channel studies where study of structure–function relationships takes a central stage. In this paper, we present a critical review of various approaches to modelling of ion transport in membrane channels, including continuum theories, Brownian dynamics, and classical and *ab initio* molecular dynamics. Strengths and weaknesses of each approach are discussed and illustrated with applications to some specific ion channels.

Contents

1. Introduction

For survival, living organisms require protection from the vagaries of chaos reigning in the outside world. At the fundamental level of single cells, this essential function is provided by the plasma membranes — mosaics composed of lipid bilayers that form a 40–80 Å thick skin around cells. Cell membranes function as selective barriers, which allow living cells to maintain an intracellular electrolyte composition that is different from that of the extracellular solution. The barrier function is maintained by the lipid bilayer, as the bilayer hydrophobic core has a low dielectric constant (2) compared to water (80), such that the transfer energy for moving ions from the aqueous solution into the bilayer core is prohibitively large. The transfer energy can be decomposed into two contributions: the ion's self-energy, due to the induced charges at the dielectric boundary between the bilayer and the aqueous solutions; and the ion's interaction energy with other charges in the system. In a bilayer the former contribution is dominant and, to a first approximation, the transfer energy can be estimated from the Born charging energy—the ion's self-energy for transfer from bulk water into a bulk hydrocarbon–which is 65 kT for an ion of radius 2 Å (Parsegian 1969). The ion concentration in the bilayer core therefore is effectively zero, which accounts for the bilayer's impermeability to small inorganic ions and other polar molecules. Membrane proteins, which catalyse the selective transfer of material and information across the plasma membrane, are remarkably effective in moving ions across biological membranes, as evident by the fact that the specific resistance of many cell membranes is about 10^3 cm^2, which is 10^6 times less than the bilayer's specific resistance (Andersen 1989a). One special class of membrane proteins, the ion channels, can affect the movement of 106 to 108 ions s^{-1} (for a given channel, the rate varies as a function of ion type and concentration, as well as the potential difference across the membrane).

The high turnover rates of ion channels, which were first described for channels incorporated into synthetic lipid bilayers (Bean *et al* 1968, Hladky and Haydon, 1970) and later for nicotinic acetylcholine-gated channels in biological membranes (Neher and Sakmann 1976), were rationalized by postulating the existence of water-filled pores through which ions could move by electrodiffusion from one aqueous phase to the other (for the historical development of the ion channel concept, see Hille 1992). Membrane-spanning proteins form the walls of these pores, and the water-filled pore together with the surrounding protein constitute the ion channels. These channels enable passive diffusion of selected ions by reducing the magnitude of their self-energy through favourable interactions, which forms the basis for selective ion permeation. The reality of biological ion channels was demonstrated by the observation of water-filled channels in electron diffraction studies of gap junction channels (Unwin and Ennis 1984) and nicotinic acetylcholine-gated channels (Toyoshima and Unwin 1988, Unwin 1995).

Ion channels are the functionally simplest among the proteins that catalyse transmembrane solute movement, in the sense that the ion movement occurs as an electrodiffusive barrier crossing, in which the passage of an ion is uncorrelated with (major) conformational changes in the channel structure. Changes in protein conformation regulate channel function, i.e. determine whether the channel is 'open' and permeable for selected ions or 'closed' and impermeable to all ions. The molecular details of the conformational changes that regulate channel function are of fundamental importance, because the high turnover number means that channel function must be tightly regulated; but we will focus only on the function of the open channels, where the challenge is to understand how a channel's ability to select among different ions, and the rate of ion movement, are determined by the molecular structure of the channel proteins. Even at this level, ion channels exhibit remarkable complexities that need to be considered when developing realistic models of ion permeation: ion channels can

discriminate among chemically similar ions, such as Na^+ and K^+; many channels bind the selected ions so strongly that a single ion will remain bound in some energy well in the pore, and the productive transport events depend on having multiple ions in the pore; and ions often move in a single file in the pore, meaning that ions cannot pass one another or even water in some cases.

Until recently, little was known about the molecular structure of the membrane proteins in biological membranes. Consequently, most modelling efforts were directed toward understanding the characteristics of ion movement in simple 'hole in the wall' type models using methods developed to understand the physical chemistry of bulk electrolyte solutions. An important conclusion of these models was that the limited dimensions of the pore could give rise to unexpected behaviours, such as flux saturation (Levitt 1986). For more realistic models, the channels formed by the antibiotic peptide gramicidin A (GA) have long been important, as they were the first channels for which an atomic resolution structure was proposed (Urry 1971) and experimentally determined (Arseniev *et al* 1986, Ketchem *et al* 1997, Townsley *et al* 2001), and their permeability properties have been studied extensively by many workers (Neher *et al* 1978, Urban *et al* 1980, Andersen 1983, Becker *et al* 1992). In fact, even though atomic resolution structures now are available for a number of channels, most importantly the bacterial potassium channel KcsA (Doyle *et al* 1998), the GA channel remains the only valence-selective channel for which there exists an atomic resolution structure of the conducting channel. Not surprisingly, therefore, GA channels have been important for developing models of ion permeation.

As new analytical methods have been developed and the available computational power increased, models of ion permeation have become increasingly sophisticated, and it is now possible to address many aspects of ion permeation using molecular dynamics (MD) simulations. These methods were originally implemented for GA channels (Roux and Karplus 1994). As atomic resolution structure of channels formed by integral membrane proteins became available (Weiss *et al* 1991, Doyle *et al* 1998, Chang *et al* 1998), this stimulated a flurry of activity in developing more detailed models of 'real' ion channels. This activity has also increasingly attracted the attention of physicists and chemists.

Having set the goalpost as elucidation of the structure–function relationships in ion channels, the next question is how one should go about it. The system in question is highly inhomogeneous, consisting of thousands of atoms in protein, lipid and water interacting among themselves and with ions via the long-range Coulomb forces. A brute force approach starting from the fundamental equations is clearly bound to fail for such a complex system even if one has access to the most powerful computers in the world. The physicists' approach to model building, that is simplifying the system to bare essentials with guidance from experimental data, offers a more amenable alternative for modelling of ion channels. As biology evolves from a descriptive to a quantitative science, methodologies used in physics and chemistry are gradually adapted to study the functional properties of biomolecular systems. In this respect, ion channels with their rich physiological background offer one of the best targets for development and testing of suitable techniques in this emerging field.

The purpose of this article is to give an overview of permeation models currently under development. The emphasis is on models that directly relate channel structure to its function, as those are of the greatest interest to physicists and chemists. Another large class of permeation models, the discrete state kinetic models (also called rate theory models) continue to be used by experimentalists in practical analysis of experimental results (Andersen 1989b); but they will not be discussed in any detail here. After a brief survey of structural and functional properties, we discuss electrostatics in a channel environment, which is the main determinant of ion dynamics. A critical review of various approaches to ion permeation in channels follows

in section 3. This section forms the essence of the review focusing on issues of consistency, relevance and feasibility. Application of these permeation models to some ion channels of biological interest is discussed in section 4.

1.1. Structural motives

Ion channels are formed by bundles of special proteins embedded in the membrane. There are two important structural determinants of channel-mediated ion permeation: the shape of the water-filled pore through which the ions move, which is defined by the geometry of the protein/water boundary; and the distribution of charges in the protein wall. The former determines the ions' self-energy and the latter, the ions' interaction energy with the channel protein. Here we give a general survey of these two features, relegating specific case studies to section 4.

The shape of a channel is influenced by two conflicting requirements. In order to conduct the maximum number of ions in a very short time, it needs to have large cross section. Yet for survival of cells, it needs to conduct ions selectively, and recognition requires a narrow profile, especially if the ions in question carry the same charge as is often the case. The compromise nature has reached is to have a relatively short and narrow segment that performs the function of selectivity filter and wider regions in the rest of the channel (figure 1). While the precise shape of a channel varies according to its type, these two characteristic regions appear to be a general feature of all biological channels. Synthetic channels do not have to satisfy the above requirements, and therefore can have more regular structures. For example, the GA channel has an approximately cylindrical shape with a radius of 2 Å, which is exceptionally narrow considering its lack of selectivity among monovalent cations.

Charge residues in the protein wall directly interact with the permeating ions, therefore their location and magnitude are of primary importance for modelling purposes. Favourable interactions can increase the concentration of certain ions in the channel and thereby enhance their conductance manyfold, while suppressing the conductance of other ions with different charge and/or size. We give an example from the KcsA potassium channel to illustrate this point: its internal volume is about 2000 $Å^3$, so that ignoring the ion–protein interactions, it would be occupied by an ion 20% of the time in a 0.15 M KCl solution. In fact, the x-ray picture shows that the KcsA channel holds three cations thanks to the high density of negative charges on its walls (Doyle *et al* 1998). Even in the GA channel which is apparently neutral, monovalent cations conduct while anions are rejected, presumably a direct result of the charge distribution in the peptide. Clearly, a fairly accurate knowledge of significant charge residues in the channel protein is essential for modelling efforts to be fruitful.

1.2. Functional properties

Ion channels serve their physiological functions by enabling the controlled (i.e. gated) movement of selected ions across biological membranes. We expand on these characteristics below. A more detailed exposition can be found in Hille (1992).

Conductance. When open, ion channels conduct current at the picoampere level (net ion fluxes on the order of 10^7 ion s^{-1}), and channel activity is 'visible' as discrete, step-like changes in the current through the membrane. Until the mid-1970s, the measurement of such small currents in cell membranes was problematic due to noise. The situation changed dramatically when Neher and Sakmann invented the patch-clamp method (Neher and Sakmann 1976), which later was improved to become the giga-seal patch-clamp method in current use (cf Hamill et al 1981). Since then, current-voltage (*I–V*) curves have been determined for numerous ion channels. In

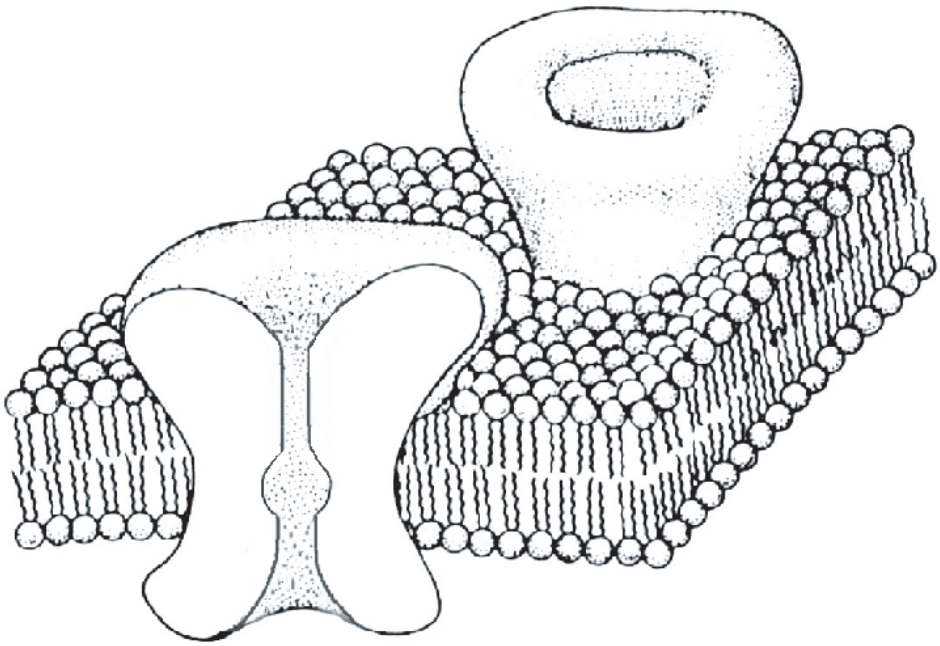

Figure 1. Cross section of a schematic ion channel embedded in membrane (modelled after the KasA potassium channel).

the physiological range of membrane potentials (-100 mV $< V <$ 50 mV), many I–V curves are linear and the single-channel conductance (G) remains one of the most prevalent descriptors of channel function. I–V curves measured under symmetrical conditions (same composition of the extracellular and intracellular solutions) may exhibit non-linearities at higher potentials, $|V| > 100$ mV (cf Andersen and Procopio 1980). These non-linearities reflect the energetics of ion permeation through the pore and studies of I–V curves can provide important insights into ion permeation (Urban *et al* 1980, Eisenman and Horn 1983, Becker *et al* 1992). It thus becomes important to have experimental information about ion permeation at as high applied potential as is technically feasible (up to 500 mV, Andersen 1983), as the deviations from linearity become more apparent at higher voltages.

Another important variable in current measurements is the concentration of the permeant ions in the baths. By measuring the single-channel current as a function of the permeant ion concentration, at a constant voltage, one obtains conductance-concentration (G–c) curves. A feature common to all ion channels is that conductance increases linearly with concentration at first but then saturates with further increase. This behaviour is traditionally described by the Michaelis–Menten function (Hille 1992)

$$G = G_{\max}/(1 + c_s/c), \tag{1}$$

where $G_{\max}$ is the maximum conductance and c_s is the saturation concentration at half-maximum. There is a great deal of variation in the measured c_s values ranging from 0.01 M for Ca channels to about 0.3 M in GA. An intuitive explanation of saturation follows from the fact that ions move across the channel in single file and need to overcome energy barriers. Thus, regardless of the bath concentrations, there is a minimal transport time for each ion to cross the channel, which translates to a maximal possible current for a given voltage. The ability of

a model to reproduce a G–c curve is much more important than fitting I–V curves, which can be achieved, for example, by simply adjusting the diffusion coefficient of ions. In contrast, there is no easy way of achieving saturation in a permeation model other than describing ion dynamics in the channel correctly. We demonstrate in section 3 how the G–c curves provide a litmus test for various models of permeation.

In the above experiments, the baths inside and outside of a cell are assumed to have the same concentration. A third class of physiological studies involves using asymmetric solutions so that there is a concentration gradient across the membrane. Again, numerous I–V curves have been obtained using asymmetric solutions. These are intrinsically more complex curves because the combination of chemical and potential gradients already creates a nonlinear behaviour, even before the ion–channel interactions are taken into account. In this case, prediction of the Nernst potential (the point where the current vanishes) would provide a relatively simple test for a model's validity.

Selectivity. The extracellular Na^+ concentration is about 10-fold higher than the intracellular Na^+ concentration, and the intracellular K^+ concentration is about 30-fold higher than the extracellular K^+ concentration— and the concentrations of both Na^+ and K^+ are much higher than those of Ca^{2+}. These concentration differences are central for normal cell physiology, as the controlled changes in membrane potential that underlie the rapid electrical signaling in nerve, muscle and heart depend on controlled changes in the permeability to K^+, Na^+ and Ca^{2+}, which give rise to the observed potential changes. It thus is necessary for ion channels to be able to discriminate among different cations—even K^+ and Na^+. It is essential for channels that conduct Ca^{2+} and K^+ to be impermeable (or have very little permeability) to Na^+, and vice versa. For potassium channels, selectivity is based on the size of ions (crystal radius of Na is 0.95 Å, and of K is 1.33 Å). The molecular structure of the selectivity filter in the KcsA channel provides a glimpse of how nature achieves this in practice (Doyle *et al* 1998). Because the filter structure appears to be conserved in all potassium channels, the specific selectivity mechanism deduced from the KcsA is likely to apply to all of them. For calcium channels, selectivity is based on charge difference. Since the tertiary structure of calcium channels is not known yet, one needs to rely on model studies to understand the selectivity mechanism in this case (Corry *et al* 2001). Anion–cation selectivity is another common feature of ion channels, and can be understood relatively easily in terms of the charge distribution in the membrane proteins. Other channels also exhibit selectivity but the permeability ratios are not as pronounced as in the above cases (Hille 1992). Understanding the selectivity sequences among ions with the same charge and predicting their permeability ratios poses the ultimate challenge to the permeation models.

Gating. The very high turnover numbers of ion channels means that their activity, whether they are open or closed, needs to be tightly controlled. The controlled changes in channel activity that are necessary for normal cell function are denoted gating, and a host of clinical diseases results from changes in the number of functional ion channels or in channel gating (Lehman-Horn and Jurkat-Rott 1999). Measurements of channel densities (number of channels/membrane area) and activation curves remain important descriptors of any ion channel.

Channel gating is not a focus of this review, but it is important to note that ion channels can be gated by changes in the potential difference across the membrane (voltage-dependent channels), by binding small chemical transmitter molecules to the channel (ligand-gated channels) and by mechanical stimulus (stretch-activated channels). In voltage-dependent channels, several charges move across the voltage sensor of the channel (Bezanilla 2000). In ligand-gated channels, differences in the binding energy of the ligand to the closed and

open channel states provides the energetic basis for channel activation (e.g. Jackson 1989). In neither case, are the molecular mechanisms resolved – except that studies on the pH-induced activation of KcsA show that proton binding causes a widening of the intracellular entrance to the channel (Perozo *et al* 1999).

1.3. Structure–function relationships

Thanks to the rapid advances summarized above, the field of ion channels has matured to a level ripe enough for serious work in model building. The goal of a model should be to come up with a theoretical framework that relates the available structural information to the observed properties of ion channels. In doing this, it should also provide an understanding for the underlying physical processes and, more importantly, be able to make predictions that could be tested experimentally. To a physicist or a chemist, these requests may appear standard for any model system, but they are hardly satisfied in most of the current model studies of ion channels. The complexity of the channel system is partly the blame, though the prevailing attitude of over-reliance on model results as an end in themselves, and neglecting to make contact with experimental data, does not help in creating a healthy environment for progress either. This is all the more ironic, given that ion channels provide one of the best biological system for studying structure–function relationships. The amount of available physiological data to be interpreted by model studies is already overwhelming. But the most exciting prospect from the viewpoint of interaction between theory and experiment is the ability to make mutations in the amino acid sequence of membrane proteins, thereby modulating the structure–function relationship with respect to the reference (native) ion channel. A celebrated example is the mutation of negatively charged glutamate residues to neutral ones in the Ca channel that led to the identification of the selectivity filter in this channel (Yang *et al* 1993). Obviously, the possibilities for random mutations are endless, and guidance from theoretical models that can predict the effect of specific mutations would be very helpful in turning such experiments into a valuable tool for exploration of the structure–function relationships in ion channels.

2. Electrostatics in channels

The forces acting on ions in and near the vicinity of a channel ultimately determine their dynamic behaviour and transport properties across the channel. A microscopic calculation of this force, even at a classical level, is made difficult because of the long-range Coulomb interactions and large dipole moment of water molecules that dominate the model system. At present, continuum electrostatics provides the only practical method for force calculations in permeation models, in the sense that it allows a reliable determination of conductance of a channel, thus enabling a direct contact with the physiological data. In this section, we discuss methods of solving Poisson's equation in a channel environment, effects of ionic atmosphere and issues concerning the validity of continuum electrostatics in narrow pores.

2.1. Solution of Poisson's equation

In continuum electrostatics, water, membrane proteins and lipid bilayer are treated as continuous media with uniform dielectric constants, typically $\varepsilon = 80$ for water and $\varepsilon = 2$ for protein and lipid. The boundary between water and protein is assumed to be sharply defined. Once the positions of fixed charges in the protein and mobile ions in water are specified with a charge density ρ, the potential φ and electric field $\boldsymbol{E}$ acting on the ions are determined from

the solution of Poisson's equation

$$\varepsilon_0 \nabla \cdot [\varepsilon(\boldsymbol{r}) \nabla \varphi(\boldsymbol{r})] = -\rho(\boldsymbol{r}), \tag{2}$$

subject to the boundary conditions

$$\varphi_1 = \varphi_2, \qquad \varepsilon_1 \nabla \varphi_1 \cdot \hat{\boldsymbol{n}} = \varepsilon_2 \nabla \varphi_2 \cdot \hat{\boldsymbol{n}}, \tag{3}$$

where $\hat{\boldsymbol{n}}$ is the unit normal to the surface and the subscripts 1 and 2 refer to the two sides of the boundary. While solving equation (2) may look menacing for many charged particles, in practice one uses the superposition principle by solving the single-charge problem for each particle and then adding all the solutions to obtain the total potential.

Methods of solution. Poisson's equation (2) separates into over a dozen coordinate systems, and if one can approximate the channel boundary with one of these coordinate systems, analytic solutions can be obtained. The only system that comes close to the boundary shown in figure 1 is that of toroidal coordinates (doughnut shape). Unfortunately, the solutions obtained using a toroidal boundary are extremely complicated (Kuyucak *et al* 1998)—so much so that conductance of the channel could not be determined from Brownian dynamics (BD) simulations even on a supercomputer (Li *et al* 1998). Thus, numerical solution of Poisson's equation remains the only alternative, especially for realistic modelling of channel boundaries. Below we briefly comment on the boundary-element and finite-difference methods developed for this purpose.

In the boundary element method (Levitt 1978), the channel boundary is divided into small segments of area s_i, and the polarization charge density σ_i on each segment is calculated from Gauss's law and the boundary conditions (3) as

$$\sigma = 2\varepsilon_0 \frac{\varepsilon_2 - \varepsilon_1}{\varepsilon_2 + \varepsilon_1} \boldsymbol{E}_{\text{ex}} \cdot \hat{\boldsymbol{n}}, \tag{4}$$

where $\boldsymbol{E}_{\text{ex}}$ is the external field due to all the charges in the system except those in s_i, which can be determined from the normal derivative of the external potential at $\boldsymbol{r}_i$

$$\varphi_{\text{ex}}(\boldsymbol{r}_i) = \frac{1}{4\pi\varepsilon_0} \left[\sum_{j \neq i} \frac{\sigma_j s_j}{|\boldsymbol{r}_i - \boldsymbol{r}_j|} + \sum_k \frac{q_k}{\varepsilon_k |\boldsymbol{r}_i - \boldsymbol{r}_k|} \right]. \tag{5}$$

Here j is summed over all the segments and k over all charges. Starting with an initial charge density of $\sigma_j = 0$, equations (4) and (5) are iterated until the results converge. By taking the curvature of segments into account, this method has been made very fast and accurate recently (Hoyles *et al* 1998b). Its only drawback is that it does not allow assignment of different ε values to channel and bulk waters because ions crossing a sharp boundary encounter infinities. Further work is needed to resolve this problem by smoothing the boundary crossing.

The finite-difference method was actually developed to solve the Poisson–Boltzmann (PB) equation for biomolecules in an electrolyte solution (Davis and McCammon 1990, Sharp and Honig 1990). By setting the ionic concentrations to zero, the same codes can also be used to solve Poisson's equation, though it has rarely been applied to ion channels in this context. In this method, the space is discretized with rectangular boxes of volume $V = h_1 h_2 h_3$. Equation (2) is integrated over the volume of each box and the lhs is converted to a surface integral using Gauss's law. Expressing the derivatives of φ as finite differences and denoting the total charge in the volume with q_i, one obtains

$$\varepsilon_0 \sum_{k=1}^{6} \varepsilon_k \frac{\varphi(\boldsymbol{r}_i + h_k \hat{\boldsymbol{k}}) - \varphi(\boldsymbol{r}_i)}{h_k} \frac{V}{h_k} = -q_i, \tag{6}$$

where the k sum is over the six neighbouring grid points with $k = 1, 2, 3$ referring to the positive x, y, z directions and $k = 4, 5, 6$, to the negative ones. Solving (6) for $\varphi(\boldsymbol{r}_i)$, one

obtains an expression relating the potential at each grid point to its six neighbours, which is solved using iterative relaxation techniques. In terms of accuracy and speed, this method is not as good as the boundary element method because iterations involve an extra dimension. Its main advantage lies in the fact that it readily allows for variations in ε values.

Applications to ion channels. The main role of Poisson's equation in permeation models is to supply the electric potentials and fields required to calculate the current. Although permeation models are indispensable in making contact with physiological data, they do not necessarily provide direct insights into the working of a channel or its permeability characteristics. Such information is more likely to be surmised from potential energy profiles where wells point to the binding sites in a channel and barriers are related to its saturation properties. This particular use of potential energy profiles will be illustrated with specific examples in section 4. Here we discuss their common features in generic ion channels.

The potential energy of an ion with charge q can be decomposed into two parts: (i) the self-energy due to the induced charges on the dielectric boundary (also known as image or reaction-field energy) and (ii) the Coulomb interaction with the charges on the channel protein. The former is proportional to q^2 while the latter goes as q, thus their valence dependence is very different—the self-energy is always repulsive while the interaction part can be either attractive or repulsive depending on the valence of q. Also, the quadratic dependence on charge means that divalent ions have to overcome self-energy barriers that are four times larger than for monovalent ions. The interaction energy depends on the specifics of charge distribution, therefore not much can be said about its general features. But the self-energy is determined solely by the channel geometry (the dielectric boundary), and it is possible to make some general remarks.

In his seminal work, Parsegian (1969) demonstrated that an ion's self-energy should be important for ion permeation across membranes. In the case of ion movement through the lipid bilayer component, the importance of the self-energy term rapidly became accepted (e.g. Andersen 1978). In the case of channel-mediated ion movement, however, the importance of the self-energy contribution has been less appreciated, despite the early contributions of Levitt (1978) and Jordan (1982). The tendency to neglect the ion self-energy may stem, in part from the success of continuum electrostatic calculations in describing the properties of macromolecules in solutions, where the self-energy term is routinely neglected. However, this is a very different problem than for channels because ions are exterior to the proteins, and not surrounded by them. To put this question into a proper perspective, we present a comparison of self-energy of an ion in two analytically solvable cases: (i) an ion at a distance r from an infinite plane boundary representing the 'outside problem' and (ii) an ion on the axis of an infinite cylinder with radius r representing the 'inside problem':

$$U_{\rm s}(\text{plane}) = \frac{1}{4\pi\varepsilon_0\varepsilon_1}\,\frac{\varepsilon_1-\varepsilon_2}{\varepsilon_1+\varepsilon_2}\,\frac{q^2}{4r}, \qquad U_{\rm s}(\text{cyl.}) \simeq \frac{1}{4\pi\varepsilon_0\varepsilon_1}\,\frac{\varepsilon_1-\varepsilon_2}{\varepsilon_2}\,\frac{q^2}{5.8\,r}. \tag{7}$$

Here, the ion is assumed to be in medium 1, and in evaluating the integral in the cylinder case, $\varepsilon_1 \gg \varepsilon_2 \approx 2$ is assumed. Using $\varepsilon_1 = 80$, $\varepsilon_2 = 2$, we obtain for a unit charge at $r = 4$ Å, $U_{\rm s}(\text{plane}) = 0.4kT$ and $U_{\rm s}(\text{cyl.}) = 12kT$. The former may be neglected compared with the ion's kinetic energy but the latter cannot. The large difference is a direct result of the induced charges on the boundary: when the planar boundary is wrapped around the ion, the total induced charge on the boundary grows by a factor of 40! We note that the self-energy problem arises directly from the finite ion charge, and that it cannot be made to disappear by appealing to the presence of other charges. This was shown already by Parsegian (1969), who demonstrated that the self-energy for transferring a cation–anion pair from water into a bulk low-dielectric constant solvent is similar to that of transferring a single ion. Repercussions of

neglecting the self-energy in continuum theories will be discussed further below.

The self-energy calculated in an infinite cylinder is much reduced when the cylinder is finite and has vestibules. The potential energy profiles for various channel shapes have been constructed from numerical solution of Poisson's equation in numerous studies: for example, Levitt (1978), Jordan (1982, 1984), Monoi (1991), Hoyles *et al* (1996); see also the review by Partenskii and Jordan (1992). The gist of such studies is that in finite cylinders the self-energy barrier drops much faster than the $1/r$ expected from equation (7). For example, for a 35 Å length cylindrical channel, compared with (7), the self-energy is reduced by a factor of 2 for $r = 2$ Å, but this reduction grows to a factor of 3 for $r = 4$ Å and 6 for $r = 8$ Å. Thus the self-energy becomes much smaller than a kT in large channels ($r > 10$ Å), and its neglect in continuum theories may be justified in such situations. Variations in ε values of protein and channel waters from the standard values of 2 and 80 have also been considered in the above studies. Protein could have larger ε_p values (2–5), which would reduce the self-energy barrier, but this is compensated by smaller ε_c for channel waters predicted from MD simulations, which could increase it considerably (Partenskii and Jordan 1992). Generally, if $\varepsilon_c < 80$, the ion's self-energy has two contributions: the self-energy due to the polarization at the pore/protein boundary, which decreases as c decreases; and the self-energy due to the polarization at the boundary between the pore and the bulk water, which can be approximated by the Born energy

$$U_B = \frac{q^2}{8\pi\varepsilon_0 R_B}\left(\frac{1}{\varepsilon_c} - \frac{1}{80}\right), \tag{8}$$

where R_B is the Born radius of ions determined from the enthalpy of hydration. The Born energy increases as ε_c decreases, and the increase in the Born energy is larger than the decrease in the self-energy due to polarization at the pore/protein boundary. In the limit of $\varepsilon_c = \varepsilon_p$, the self-energy becomes entirely due to the Born energy. Recalling that channels were proposed to overcome the Born energy barrier posed by cell membranes, one can see why low ε_c values cannot yield a working model of permeation.

2.2. Influence of ionic atmosphere

Solution of Poisson's equation provides static potential energy profiles with ions at fixed positions. In an electrolyte solution, screening effects due to counter-ions exponentially dampen the Coulomb field of an ion. Whether such screening effects have a similar influence on the calculated static potential profiles in channels has important ramifications for continuum theories and therefore needs to be discussed in some detail. If the modifications are substantial, this would render the static profiles obtained from Poisson's equation more or less useless. This question was addressed by Levitt (1985), Jordan *et al* (1989) and Cai and Jordan (1990), who applied the PB theory to schematic ion channels, and their results were affirmative with regard to the importance of including the ionic atmosphere. Since then the PB equation has replaced Poisson's equation in potential calculations in numerous studies of ion channels (e.g. Sankararamakrishnan *et al* (1996), Weetman *et al* (1997), Adcock *et al* (1998, 2000), Cheng *et al* (1998), Rostovtseva *et al* (1998), Sansom *et al* (1998), Dieckmann *et al* (1999), Ranatunga *et al* (1999)). This view has recently been challenged by Moy *et al* (2000), who showed through comparisons with BD simulations that the PB theory breaks down in narrow pores because it fails to take the self-energy contributions into account. After a brief review of the PB theory, we discuss these new developments below.

Poisson–Boltzmann equation. PB theory provides a continuum description of a system in which fixed external charges, represented by a density ρ_{ex}, are surrounded by mobile ions of

density ρ_{el} in a dielectric medium. The main assumption of the theory is that at equilibrium, the distribution of mobile ions in the system is given by the Boltzmann factor

$$\rho_{el}(\boldsymbol{r}) = \sum_{\nu} z_\nu e n_{0\nu} \exp\left[-z_\nu e\varphi(\boldsymbol{r})/kT\right], \tag{9}$$

where $n_{0\nu}$ is the bulk (or reference) number density of ions of species ν and $z_\nu e$ is their charge. Here n_0 (in SI units) is related to concentration c_0 (in mol l^{-1}) by $n_0 = 1000 N_A c_0$ where N_A is Avogadro's number. Substituting the charge density (9) in Poisson's equation (2), one obtains the PB equation for a $z{:}z$ electrolyte

$$\varepsilon_0 \nabla \cdot [\varepsilon(\boldsymbol{r})\nabla\varphi(\boldsymbol{r})] = 2ezn_0 \sinh\left[ze\varphi(\boldsymbol{r})/kT\right] - \rho_{ex}. \tag{10}$$

In practical applications, the PB equation is solved numerically using a finite-difference method similar to the one described for Poisson's equation in the last section. In fact, the equation employed in PB iterations can be simply obtained from (6) by substituting $q_i \to q_i - 2ezn_0 \sinh[ze\varphi(\boldsymbol{r}_i)/kT]V$.

There are only a few known analytical solutions of equation (10), all involving infinite boundaries (for example, the Gouy and Chapman theory for a plane), and therefore not very relevant for channels. A more useful example for our purposes is that of a central ion in a bulk electrolyte, first solved by Debye and Hückel by linearizing the PB equation

$$\nabla^2\varphi = \kappa^2\varphi, \qquad \kappa^{-1} = \sqrt{\frac{\varepsilon_0 \varepsilon kT}{2z^2e^2n_0}}. \tag{11}$$

Here κ^{-1} is the Debye screening length and $\rho_{ex} = 0$. Solution of (11) yields the following screened Coulomb potential around a central ion of radius $a/2$ (for example, McQuarrie (1976))

$$\varphi = \frac{ze\,\mathrm{e}^{-\kappa(r-a)}}{4\pi\varepsilon_0\varepsilon(1+\kappa a)r}. \tag{12}$$

The radial density of the screening charge $P(r)$ is proportional to this potential

$$P(r) = 4\pi r^2\rho_{el} = -4\pi r^2\varepsilon_0\varepsilon\kappa^2\varphi = \frac{-ze\kappa^2}{1+\kappa a}\, r\mathrm{e}^{-\kappa(r-a)}, \tag{13}$$

which is seen to peak at $r = \kappa^{-1}$ and then decay exponentially. The volume integral of this shielding charge for a sphere of radius r is given by

$$Q(r) = -ze\left[1 - \frac{1+\kappa r}{1+\kappa a}\,\mathrm{e}^{-\kappa(r-a)}\right]. \tag{14}$$

Equation (14) shows that $-Q(r)/ze$ increases monotonically with r, leading to a 25% screening of the central charge at about $r = \kappa^{-1}$, rising to 90% at $r = 4\kappa^{-1}$. At room temperature ($T = 298$ K) and in water, Debye screening length is related to concentration as $\kappa^{-1} = 3.07/(z\sqrt{c_0})$ Å, so that at the physiological $c_0 = 0.15$ M, $\kappa^{-1} = 7.9$ Å. Thus, near-complete screening of an ionic charge occurs at a length scale of about 30 Å, and the volume in question ($\sim 10^5$ Å^3) contains ten counter-ions and nine co-ions. Ion channels have volumes typically two orders of magnitude smaller and contain only a few ions at a time. It is difficult to visualize how the screening effects predicted by the PB calculations could take place in reality. Yet the success of the PB theory in applications to macromolecules (Davis and McCammon 1990, Sharp and Honig 1990) was deemed sufficient proof for its validity in channels. Framing of the theory in terms of concentration rather than particles has doubtless obscured this problem, delaying its identification for a long time. Only by thinking in terms of particles and forces has it become intuitively obvious.

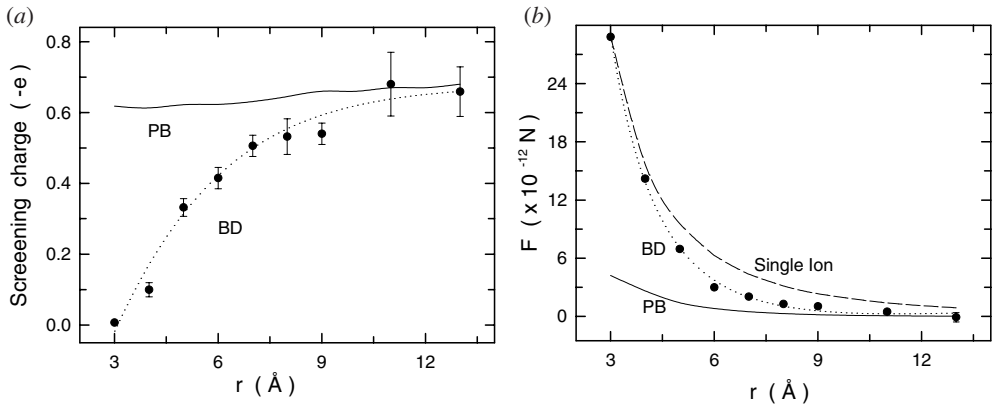

Figure 2. Comparison of the net screening charge in the channel (*a*) and the force on a test ion (*b*) in the PB and BD approaches as a function of the channel radius. The cation is held at $z = 12.5$ Å from the centre of the channel. The dashed curve indicates the single-ion results obtained from Poisson's equation.

Test of PB theory in channels. The PB theory was tested in channels by comparing its predictions for force on a test cation with those obtained from the BD simulations (Moy *et al* 2000). A cylindrical channel with length 35 Å and a variable radius was used with a 0.3 M NaCl solution ($\kappa^{-1} = 5.6$ Å). The PB equation was solved using a finite-difference method similar to the one used for Poisson's equation (6). Details of the BD method is given in the next section. The main results of this study are summarized in figure 2, which compares the net screening charge in the channel (*a*) and the force on the ion (*b*) in the PB and BD approaches. Because of the large self-energy barriers in narrow pores (e.g., $4kT$ for $r = 4$ Å), anions cannot enter the channel in BD, and thus there is no shielding of the test cation (note that the BD results overlap with those of a single ion). With increasing radius, self-energy goes down, anions start entering the channel in increasing quantities and thereby provide some shielding, as attested by the reduction of the force in BD from that of a single ion. In contrast, the PB results predict a significant shielding effect regardless of the size of the channel. Discrepancy is worst in narrow pores where screening leads to a fivefold reduction in force as compared with BD. Near-constancy of the net screening charge is a direct consequence of neglect of the self-energy in PB theory. Inspection of the numerical solutions shows that each grid point contains a tiny fraction of a unit charge. The self-energy associated with such a small charge, recalling that it is proportional to charge squared, is truly negligible. When ions are treated as particles rather than a continuous charge distribution, they feel the full brunt of the self-energy barrier and fail to enter the channel. In larger pores, the self-energy of ions becomes quite small so that errors committed in PB are negligible, and the PB and BD results merge. Convergence occurs at a radius of two Debye lengths, which gives a rule of thumb for the domain of validity of the continuum theories in channels.

Returning to the question posed at the beginning of this section, the BD simulations clearly show that inclusion of the ionic atmosphere has no influence on the potential energy profiles obtained from Poisson's equation in narrow pores ($r < 5$ Å). Therefore such profiles can be safely used to make inferences about a channel's permeation properties. Application of the PB theory to narrow pores, on the other hand, is highly problematic due to neglect of the self-energy. This problem needs to be addressed before the PB theory can be reliably used for calculation of potential profiles or pK_A values of ionizable charge residues in channels.

2.3. Appraisal of continuum electrostatics in channels

Continuum electrostatics provides a valid description of macroscopic dielectric media because averaging of fields is done over a very large number of atoms and the atomic details are washed out. Its success in describing properties of biological macromolecules (Warshel and Åqvist 1991, Honig and Nicholls 1995) shows that it can also be used in mesoscopic systems profitably provided that the macromolecule–solvent interface is properly modelled. Ion channels lie in a grey area between microscopic and mesoscopic systems in that their radial dimensions and solvent accessible volumes could be quite small. Microscopic studies of water confined in small volumes indicate that the boundary imposes an order on the neighbouring water molecules reducing their polarizability substantially (Zhang *et al* 1995, Sansom *et al* 1996, 1997, Green and Lu 1997, Tieleman and Berendsen 1998, Allen *et al* 1999a). As a result, one expects the dielectric response in a channel to be both position and direction dependent, and the ε values to be much suppressed as compared with the bulk. Use of a non-uniform dielectric tensor instead of a uniform ε does not pose any technical difficulties as it can be easily implemented in a finite-difference algorithm. What is not clear is whether such a quantity can be reliably estimated from a microscopic method such as MD simulation. In fact, the whole issue of microscopic validation of continuum electrostatics in channels remains an outstanding problem that needs to be explored further.

In the face of such uncertainties, the practical response of permeation modellers has been to use a uniform ε value in the channel. It is important to emphasize that such an effective ε value does not represent the polarizability of channel waters in response to some external field, which could be quite low as the MD simulations demonstrate, but in fact, has little relevance on the dynamics of permeating ions. Rather it reflects the effectiveness of water molecules around an ion in screening its charge. In continuum electrostatics, this screening is attributed to the first hydration shell, and the success of the Born model in correlating experimental solvation energies lends phenomenological support for this interpretation. Recent MD free-energy calculations of solvent charge distribution around an ion and solvation energies have provided further microscopic support for the primacy of the first hydration shell (Roux *et al* 2000). Because the electric field of an ion in its first hydration shell is much stronger than that of any other source, one expects it to dominate the solvation dynamics regardless of whether the ion is in bulk or in a channel environment. Thus, as long as the first hydration shell of ions remains intact in a channel, use of continuum electrostatics with a bulk-like ε value can be justified. This criterion is generally satisfied in ion channels, including the narrow selectivity filter regions where protein atoms substitute for water completing the solvation shell. The only exception found so far is the GA channel, in which water and ions move in single file for the entire length of the pore. Using both theoretical and experimental arguments, one can show that continuum electrostatics completely fails in this case, as discussed in more detail in section 4.1.

3. Theories of permeation

Before moving into theories of ion permeation in channels it is worth summarizing the current state of affairs in bulk electrolytes (Bockris and Reddy 1970). At a phenomenological level, Ohm's and Fick's laws or their combination, the Nernst–Planck (NP) equation, provide an adequate description of the conductance properties of electrolyte solutions. At this level, diffusion coefficient or conductivity of ions are parameters that are taken from experiments. A great deal of effort went into trying to relate these parameters to molecular properties of electrolytes during the last century. However, not much progress has been made towards this

goal, indicating the difficulty of the problem. One notable exception is Onsager's prediction of $\sqrt{c}$ dependence of conductivity on concentration in dilute electrolytes. Otherwise, there is still no microscopic theory that can explain, for example, the exponential increase of conductivity with temperature. Computational approaches such as MD simulations provide insights on the key role played by hydration shells of ions but lack the predictive power required for a quantitative understanding. Considering the fundamental role temperature plays in statistical mechanics, this is far from being satisfactory and certainly limits the utility of electrolyte theories when applied to other areas. Because ion channel studies are almost always carried out at room temperature, neither potential rewards of experimental investigation of temperature dependence of conductance nor difficulties associated with its theoretical interpretation seem to be well appreciated in the field (Kuyucak and Chung 1994, Chung and Kuyucak 1995). Hopefully this situation will change once the permeation models are perfected and become more predictive.

Given the tenuous state of theory in bulk electrolytes, there is little point in trying to model ion permeation in channels using sophisticated methods unless they are proven to be absolutely necessary. The only prerequisite for any proposed model is that it should describe the ion–channel interactions sufficiently accurately. Thus, in the following, we will proceed from the simplest continuum theories to the more involved BD and MD simulations, stressing at each stage why the next level of complexity is required. We will not discuss the reaction rate theory (or barrier model) approach because our emphasis is on the relationship between channel structure and ion permeation. Even though barrier models can provide insights into ion–ion interactions or summarize a channel's permeability properties concisely (Urban *et al* 1980, Becker *et al* 1992, McCleskey 1999, Miller 1999), the model parameters have no direct physical relation to the channel structure (Andersen 1989b, Levitt 1999, Nonner *et al* 1999). It is not possible, for example, to relate the estimated value of a rate constant to the height of the energy barrier the ion is traversing (Andersen 1989b, Andersen and Koeppe 1992). That said, if it is possible to decompose the overall ion transfer through the channel into a few discrete steps, one may be able to use continuum models to relate the rate constants to the channel structure (e.g. Andersen 1989b)—which could simplify the task of 'debugging' continuum descriptions of ion permeation.

3.1. Continuum theories

Continuum theories of permeation were proposed as more realistic alternatives to rate theories in the mid-1980s and their application to ion channels have flourished since then (see Levitt (1986), Cooper *et al* (1988), Hille (1992), Eisenberg (1996, 1999) for reviews and earlier references; more recent references are Nonner and Eisenberg (1998), Nonner *et al* (1998, 1999, 2000), Kurnikova *et al* (1999), Cardenas *et al* (2000), Hollerbach *et al* (2000), Adcock *et al* (2000)). Being the simplest permeation theories that allow incorporation of channel structure, the NP and Poisson–Nernst–Planck (PNP) equations are the first candidates to consider in modelling of ion channels. After giving a brief account of the formalism, we discuss the crucial question of whether the ion–channel interactions are properly taken into account in continuum theories of permeation.

Poisson–Nernst–Planck equations. In continuum theories, the flux $\boldsymbol{J}_\nu$ of each ion species is described by the NP equation which combines the diffusion due to a concentration gradient with that from a potential gradient

$$\boldsymbol{J}_\nu = -D_\nu \left(\nabla n_\nu + \frac{z_\nu e n_\nu}{kT} \nabla \varphi \right), \tag{15}$$

where n_ν is the number density and D_ν is the diffusion coefficient of the ions of species ν, and

we have used the Einstein relation $\sigma = (zen/kT)D$ to express the conductivity in terms of the diffusion coefficient. In some applications, the NP equation (15) is solved with potentials determined from the solution of the PB equation (10) or simply with an assumed profile. Clearly this is not a self-consistent procedure, and the potential should be determined from the solution of Poisson's equation (2) using the charge density $\rho = \sum_\nu z_\nu e n_\nu + \rho_{\rm ex}$, where the two terms represent the mobile ions and the external charges as before. In the PNP theory, equations (2) and (15) are solved simultaneously, yielding the potential, concentration and flux of ions in the system. Numerical solutions are obtained using a finite-difference method as in Poisson's or the PB equation. Poisson's equation (6) is modified with the substitution $q_i \to q_i + V\sum_\nu z_\nu e n_\nu(\boldsymbol{r}_i)$, which yields an expression relating the central potential at $\boldsymbol{r}_i$ to its immediate neighbours. Similarly, the flux through the surfaces of the rectangular box at $\boldsymbol{r}_i$ is discretized using the NP equation (15) as follows:

$$J_k = -D\left[\frac{n_k - n_i}{h_k} + \frac{ze}{kT}\frac{1}{2}(n_k + n_i)\frac{\phi_k - \phi_i}{h_k}\right], \tag{16}$$

where the subscript ν is suppressed for convenience and i and k refer to the grid positions $\boldsymbol{r}_i$ and $\boldsymbol{r}_i + h_k\hat{\boldsymbol{k}}$. Using the steady-state condition $\nabla\cdot\boldsymbol{J} = 0$, one eliminates the flux dependence in (16), obtaining an expression for the central density in terms of its immediate neighbours. These two equations are iterated simultaneously, subject to the specified boundary conditions (Kurnikova *et al* 1999, Corry *et al* 2000a).

Due to their nonlinear nature, the PNP equations are notoriously difficult to solve analytically except in some very special cases: for example, the classic Goldman–Hodgkin–Katz equation (Hille 1992), and the high-field limits (Syganow and von Kitzing 1999a, 1999b). Here we discuss some of the basic formalism to indicate these difficulties, which will offer some hints as to why the problems in applications of the PNP theory to channels remained hidden for so long. As in the case of the PB equation, the strategy is to eliminate the density dependence of ions from Poisson's equation using (15). Because equation (15) is itself a differential equation, this process is somewhat more complicated. When $\boldsymbol{J}_\nu = 0$ in (15), the PNP equations trivially reduce to the PB equation with the density given by the Boltzmann factor

$$n_\nu = n_{0\nu}\mathrm{e}^{-\psi_\nu}, \qquad \psi_\nu = z_\nu e\varphi/kT, \tag{17}$$

where ψ_ν is the potential energy expressed in a dimensionless form. Using equation (17) for n_ν as an integrating factor in (15), it can be recast into the form

$$\boldsymbol{J}_\nu = -D_\nu \mathrm{e}^{-\psi_\nu}\nabla\left(n_\nu \mathrm{e}^{\psi_\nu}\right). \tag{18}$$

Under steady-state conditions and assuming only the z component J_ν is non-zero, equation (18) reduces to 1D and can be integrated between the boundary points $[0, L]$ to give

$$J_\nu = -D_\nu \frac{n_{\nu L}\mathrm{e}^{\psi_{\nu L}} - n_{\nu 0}\mathrm{e}^{\psi_{\nu 0}}}{\int_0^L \mathrm{e}^{\psi_\nu(z)}\,\mathrm{d}z}, \tag{19}$$

where the subscripts 0 and L in n_ν and ψ_ν refer to their values at the boundaries. Doing the same integration from $[0, z]$, and using (19) to eliminate J_ν/D_ν gives an expression for the ion density in terms of the potential

$$n_\nu(z) = \mathrm{e}^{-\psi_\nu}\left[n_{\nu 0}\mathrm{e}^{\psi_{\nu 0}} + \left(n_{\nu L}\mathrm{e}^{\psi_{\nu L}} - n_{\nu 0}\mathrm{e}^{\psi_{\nu 0}}\right)\frac{\int_0^z \mathrm{e}^{\psi_\nu(z)}\,\mathrm{d}z}{\int_0^L \mathrm{e}^{\psi_\nu(z)}\,\mathrm{d}z}\right]. \tag{20}$$

Finally, substituting (20) in Poisson's equation, one obtains an integro-differential equation for the potential in PNP

$$\varepsilon_0\frac{\mathrm{d}}{\mathrm{d}z}\left[\varepsilon\frac{\mathrm{d}}{\mathrm{d}z}\varphi(z)\right] = -\sum_\nu z_\nu e\mathrm{e}^{-\psi_\nu}\left[n_{\nu 0}\mathrm{e}^{\psi_{\nu 0}} + \left(n_{\nu L}\mathrm{e}^{\psi_{\nu L}} - n_{\nu 0}\mathrm{e}^{\psi_{\nu 0}}\right)\frac{\int_0^z \mathrm{e}^{\psi_\nu(z)}\,\mathrm{d}z}{\int_0^L \mathrm{e}^{\psi_\nu(z)}\,\mathrm{d}z}\right] - \rho_{\rm ex}. \tag{21}$$

This is similar in form to the PB equation, and reduces to it when $n_{\nu L}e^{\psi_{\nu L}} = n_{\nu 0}e^{\psi_{\nu 0}}$: that is, when the electrochemical forces balance out and the system is in equilibrium. In general, there are no known analytical solutions of equation (21). The main difficulty lies with the evaluation of the integrals—the only known integral of $\int e^{f(z)}\,dz$ is for $f = z$, which simply gives back e^z. This corresponds to the constant electric field approximation in the Goldman–Hodgkin–Katz theory. Using $\psi_\nu(z) = \psi_{\nu 0} + (\psi_{\nu L} - \psi_{\nu 0})z/L$ in equations (19) and (20) yields the following solutions for the flux and density:

$$J_\nu = -\frac{D_\nu}{L}\,\frac{(\psi_{\nu L} - \psi_{\nu 0})(n_{\nu L}e^{\psi_{\nu L}} - n_{\nu 0}e^{\psi_{\nu 0}})}{e^{\psi_{\nu L}} - e^{\psi_{\nu 0}}}, \tag{22}$$

$$n_\nu(z) = e^{-\psi_\nu(z)}\left[n_{\nu 0}e^{\psi_{\nu 0}} + \left(n_{\nu L}e^{\psi_{\nu L}} - n_{\nu 0}e^{\psi_{\nu 0}}\right)\frac{e^{\psi_\nu(z)} - e^{\psi_{\nu 0}}}{e^{\psi_{\nu L}} - e^{\psi_{\nu 0}}}\right]. \tag{23}$$

The effect of the electrochemical forces on density, which is not so easy to surmise from equation (20), can be seen more clearly from (23): the density, which varies linearly between the boundary values when there are no electric forces (Fick's law), exhibits an exponential behaviour when there is a uniform field. Thus the local potential has a significant effect on the cation and anion densities similar to the PB theory. It is important to emphasize that, despite their popularity, these solutions are only valid for bulk solutions and have little relevance for ion channels because the ion–channel interactions are completely ignored.

In the absence of analytical solutions, applications of the PNP theory to ion channels have been carried out using numerical methods. The 'black box' approach adapted in these applications emphasizes agreement with physiological data by fitting the model parameters but has little to say about the actual dynamics of ions, offering virtually no insights into the permeation process. It is difficult to surmise from the numerical solutions of the PNP equations whether the ion–channel interactions are correctly taken into account. As in the case of the PB theory, comparison of the PNP results with those of the BD simulations provides a straightforward test to check the validity of the PNP approach in channels.

Test of PNP theory in channels. Both the ion concentration and flux are described by continuous quantities in PNP corresponding to macroscopic, space–time averages of microscopic motion of individual ions. We have seen in the equilibrium case of the PB theory that this averaging is valid in large channels with radius greater than 2 Debye lengths and fails in narrower pores. In a conducting situation, ions diffuse at a small fraction of their thermal velocity. Thus diffusion of ions is an adiabatic process compared with their thermal motion, and the instantaneous screening of an ion as predicted by the PB theory should remain intact to a good approximation. Recalling that the problem with the PB theory is overshielding due to the neglect of self-energy, one expects PNP to suffer from the same predicament. In fact, the problem is worse here because there is at least some trace of self-energy for a test ion in PB, whereas the complete smearing of the ion charges in PNP leads to a total neglect of self-energy.

These assertions were given a solid ground in detailed tests, where PNP predictions for conductance and concentration in model channels were compared with those obtained from the BD simulations (Corry *et al* 2000a). The main concern of neglect of self-energy is illustrated in figure 3. The channel system used in calculations is the same as in figure 2. In (*a*), the self-energy contribution is switched off by setting the dielectric constant of the protein to 80, the same as for water. There is a general agreement between the two approaches at all radii. A very different picture emerges in (*b*), where $\varepsilon = 2$ is used for the protein. In BD, conductance nearly vanishes for the narrowest pores because ions cannot enter the channel due the self-energy barrier. In contrast, conductance in PNP remains at the same level as in the left panel, clearly demonstrating the neglect of self-energy in PNP. Only when the radius is larger than

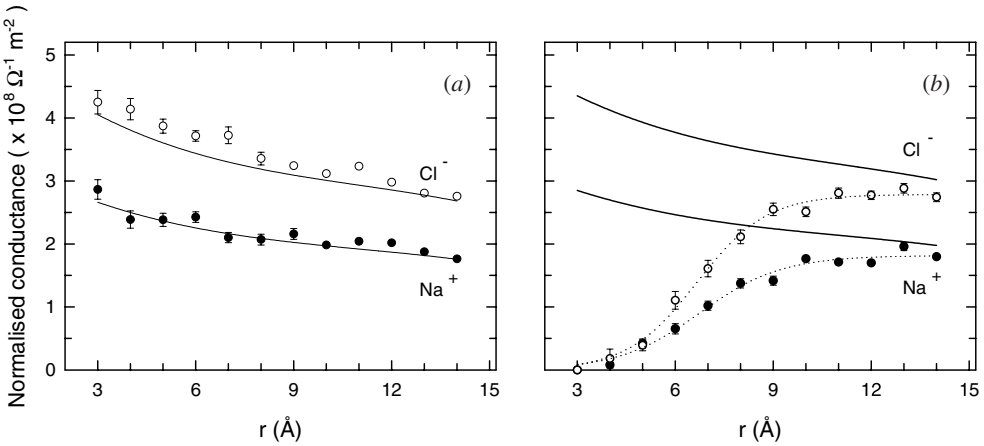

Figure 3. Comparison of conductance of Na and Cl ions predicted by PNP (solid curves) and BD (circles fitted by dotted curves) in cylindrical channels with a varying radius. The conductance values are normalized by dividing with the cross-sectional area. A symmetric NaCl solution of 0.3 M and an applied potential of 0.1 V are used. (*a*) ε for the channel protein is set to 80 so that there is no self-energy barrier for ions. The realistic case with $\varepsilon = 2$ is shown in (*b*).

two Debye lengths does the self-energy contribution become negligible, and the PNP and BD results converge. Similar results are obtained for concentration profiles of ions in the channel. In BD, self-energy barrier leads to a suppression of ionic concentration in narrow channels by more than an order of magnitude as compared with the bath values, whereas in PNP, the channel is occupied by Na and Cl ions at the bath concentrations regardless of the pore radius or ε value used for the protein.

The above test was deliberately carried out in a neutral channel to isolate the self-energy contribution from other terms in the potential energy. Tests in negatively charged channels show that convergence of cation current in PNP and BD occurs at a smaller radius, indicating that ion-fixed charge interactions are modelled correctly and help to reduce the discrepancy. On the other hand, the disagreement in anion current persists as before, and has to be suppressed by artificial means (e.g. reducing the diffusion coefficient of anions relative to cations) in order to obtain agreement with experimental data. Only in very highly charged channels, such as the KcsA potassium, does the anion current cease to flow. However, such channels are occupied by multiple ions, which gives rise to another problem in PNP, namely how to incorporate the Coulomb forces among ions in a continuum model.

As a final test of PNP, we consider the conductance–concentration curves, which should exhibit saturation as stressed in section 2.2. In all the *G*–*c* curves calculated from PNP, conductance increases linearly with concentration with no sign of saturation, regardless of the channel size or whether it is neutral or highly charged (Corry *et al* 2000a). Since the diffusion coefficients of ions are held constant and electroneutrality is maintained in PNP, this can happen only if both cation and anion concentrations in the channel rise in tandem with the bath values. Indeed this has been observed to be the case in all test calculations, including the KcsA potassium channel. Needless to say, saturation does occur in channels because counter-ions cannot enter them, which brings us back to the self-energy problem.

It is not clear whether the self-energy problem in continuum theories can be fixed in a rigorous way. Obviously, one has to give up self-consistency since that is part of the problem. A second difficulty for continuum theories is how to deal with the ion–ion interactions in multi-

ion channels, which appears to play a significant role in permeation dynamics. Until these issues are resolved, application of PNP to ion channels will remain doubtful, no matter how successful it may be in fitting experimental I–V curves. In the meantime, earnest modelling of ion channels has to be carried out using permeation theories that treat the ions in the system as discrete particles.

3.2. Brownian dynamics

The simplest permeation theory that treats ions as particles is BD, first proposed by Einstein in 1905 to describe the motion of colloidal particles in a solution. BD simulations have been used to study the influence of ions around globular proteins (e.g., Madura *etal* 1995), and the promise of BD in modelling ion channels was emphasized in an early review by Coopet *et al* (1985). But apart from a few 1D studies of model channels (Jakobsson and Chiu 1987, Bek and Jakobsson 1994), this proposal was mostly overlooked until recently. The main reason for this neglect appears to be the technical difficulties in extending BD simulations to 3D, which is necessary for realistic applications. During a typical BD simulation, Poisson's equation needs to be solved at each time step to determine the forces acting on ions, and this process is repeated millions of times. The computational overhead associated with numerical solution of Poisson's equation is fairly large, putting practical application of BD to channels in such a straightforward manner beyond the reach of even supercomputers. Not surprisingly, the first 3D BD simulation was carried out in a toroidal channel, which allows analytical solution of Poisson's equation (Li *et al* 1998). For a general channel boundary, this problem was overcome by storing the precalculated values of the electric field and potential in a system of lookup tables, and interpolating the required values from these tables during simulations (Hoyles *et al* 1998a). This innovation enabled application of 3D BD simulations to a number ion channels: e.g. acetylcholine receptor (Chung *et al* 1998), KcsA potassium (Chung *et al* 1999, 2001), L-type calcium (Corry *et al* 2000a, 2001) and GA (Edwards *et al* 2001). There are also some 3D BD studies of the porin channel (Schirmer and Phale 1999, Im *et al* 2000). However, the reaction field is ignored in these studies so that they are free from the difficulties arising from the solution of Poisson's equation. Below we discuss the Langevin equation and its implementation in BD simulations of channels.

Langevin equation. In BD simulations, the trajectory of each ion in a system of N ions is followed using the Langevin equation (Chandrasekhar 1943)

$$m_i \frac{\mathrm{d}\boldsymbol{v}_i}{\mathrm{d}t} = -m_i \gamma_i \boldsymbol{v}_i + \boldsymbol{R}_i + \boldsymbol{F}_i, \qquad i = 1, \ldots, N, \tag{24}$$

where m_i, $\boldsymbol{v}_i$ and γ_i are the mass, velocity and the friction coefficient of the ith ion. The three force terms on the rhs of (24) correspond to the frictional, random and the total systematic forces acting on the ion. The frictional and random forces represent the incessant collisions of the ion with the surrounding water molecules in an average way. Because they arise from the same source, the two forces are not independent but intimately related through the fluctuation–dissipation theorem (Kubo 1966)

$$m_i \gamma_i = \frac{1}{2kT} \int_{-\infty}^{\infty} \langle R_{ik}(0) R_{ik}(t) \rangle \, \mathrm{d}t, \qquad k = x, y, z. \tag{25}$$

Here the quantity in the integrand is the autocorrelation function of the random force and the angular brackets denote average over an equilibrium ensemble. In order to give an intuitive feeling about their role in ion permeation, we discuss the frictional and random forces in some detail below.

Table 1. Basic properties of physiologically important ions in electrolyte solutions (Hille 1992). Here r is Pauling's crystal radius, $\bar{v}$ is the average thermal speed, γ^{-1} is the relaxation time constant and ΔH is the hydration energy of ions. Note that $1kT = 4.11 \times 10^{-21}$ J at room temperature $T = 298$ K.

Ion	m (10^{-26} kg)	r (Å)	$\bar{v}$ (m s^{-1})	D (10^{-9} m^2 s^{-1})	γ^{-1} (fs)	ΔH (kT)
Na^+	3.8	0.95	570	1.33	12	−177
K^+	6.5	1.33	435	1.96	31	−144
Ca^{2+}	6.6	0.99	432	0.79	13	−671
Cl^-	5.9	1.81	473	2.03	29	−139

When $\boldsymbol{R} = \boldsymbol{F} = 0$, equation (24) has the trivial solution $\boldsymbol{v} = \boldsymbol{v}_0 e^{-\gamma t}$. Thus the friction alone would grind the motion of an ion to a halt with a relaxation time constant of γ^{-1}. Using the Einstein relation $D = kT/m\gamma$, we calculate the relaxation times for some ions of interest from their observed diffusion coefficients (see table 1). At tens of femtoseconds, the relaxation times of ions are indeed extremely short—an ion would travel about a tenth of an ångstrom in that time interval. This illustrates the essentially diffusive nature of ion permeation in water. For future reference, note that the average frictional force, estimated from the table entries, is about 1–2 nN.

The random force, by definition, has a zero mean, $\langle R_i \rangle = 0$, has no correlations with prior velocities, $\langle v_i(0) R_j(t) \rangle = 0$, and is Markovian, that is, there are no correlations with earlier times or other components (here i and j run over $1, \ldots, 3N$)

$$\langle R_i(0) R_j(t) \rangle = 2m_i \gamma_i kT \delta_{ij} \delta(t). \tag{26}$$

It is standard to assume a Gaussian probability distribution for the random force

$$w(R_i) = (2\pi \langle R_i^2 \rangle)^{-1/2} \exp(-R_i^2 / 2\langle R_i^2 \rangle), \tag{27}$$

which follows from the likewise distribution of velocities (Chandrasekhar 1943), and can also be verified directly from MD simulations (Rey *et al* 1992). Replacing the ensemble average by time average, the width of the Gaussian distribution in (27) can be calculated from (26) as $\langle R_i^2 \rangle = 2m_i \gamma_i kT/\Delta t$, where Δt is the time step used in integration of the Langevin equation. Using the entries from table 1 with $\Delta t = \gamma_i^{-1}$, the average random force is seen to be about 1–2 nN, the same range as the frictional force.

Strictly speaking, the Markovian assumption is justified when the Brownian particle is much heavier than the solvent molecules. This assumption is relaxed in the generalized Langevin equation (Kubo 1966), which is obtained from equation (24) by replacing the constant friction coefficient with a time-dependent friction kernel: that is, $m\gamma \boldsymbol{v} \rightarrow m \int_0^t \xi(t-t') \boldsymbol{v}(t')\, dt'$. The fluctuation–dissipation theorem (26) then becomes $\langle R_i(0) R_j(t) \rangle = 2m_i kT \delta_{ij} \xi(t)$. The generalized Langevin equation reduces to the Markovian one for $\xi = \gamma \delta(t - t')$. This higher level of complexity appears to be required for detailed description of equilibrium properties of electrolytes (Rey *et al* 1992), but so far it has not been considered in transport problems, presumably because the ions' motion is severely damped. We, therefore, leave the possible effects of the generalized Langevin equation as a future problem and restrict ourselves to a discussion of the Markovian one in this review.

In contrast to the frictional force, the random force keeps ions in constant agitation. As it is white, it cannot cause a drift on an ion's position on average: that is, $\langle x \rangle$, $\langle y \rangle$ and $\langle z \rangle$ remain constant when $\boldsymbol{F} = 0$. But because of fluctuations, the mean-square displacement of ions will not vanish. To see this effect of the random force on ions' motion, consider the Langevin equation (24) with $\boldsymbol{F} = 0$. Since there is no correlation between the components of

$\boldsymbol{R}$, the same equation applies in each direction: e.g. $\ddot{x} = -\gamma\dot{x} + R_x/m$, where dots indicate the time derivatives. To integrate this equation (i) multiply both sides by x, (ii) substitute $x\ddot{x} = \frac{\mathrm{d}}{\mathrm{d}t}(x\dot{x}) - \dot{x}^2$ and (iii) take the ensemble average and replace $\langle\dot{x}^2\rangle = kT/m$ from the equipartition theorem and $\langle xR_x\rangle = \langle x\rangle\langle R_x\rangle = 0$, yielding

$$\frac{\mathrm{d}}{\mathrm{d}t}\langle x\dot{x}\rangle = -\gamma\langle x\dot{x}\rangle + kT/m. \tag{28}$$

Assuming $x = 0$ at $t = 0$, (28) can be integrated to give $\langle x\dot{x}\rangle = (kT/m\gamma)(1 - \mathrm{e}^{-\gamma t})$. Finally, using $\frac{\mathrm{d}}{\mathrm{d}t}\langle x^2\rangle = 2\langle x\dot{x}\rangle$, and integrating once more, we obtain for the mean-square displacement

$$\langle x^2\rangle = (2kT/m\gamma)\big[t - \gamma^{-1}(1 - \mathrm{e}^{-\gamma t})\big]. \tag{29}$$

Two time regimes can be identified in equation (29):

(i) $t \ll \gamma^{-1} \rightarrow \langle x^2\rangle = (kT/m)t^2$, ions move ballistically between collisions with an average velocity of $\bar{v}_x = (kT/m)^{1/2}$.

(ii) $t \gg \gamma^{-1} \rightarrow \langle x^2\rangle = (2kT/m\gamma)t$, fluctuations in an ion's position grows with time just like in Fick's law for self-diffusion, $\langle x^2\rangle = 2Dt$. Thus, in the absence of systematic forces, the Langevin equation reproduces Fick's law and provides an expression for the diffusion coefficient (Einstein relation).

The above equilibrium picture of ions is disturbed once systematic forces are in operation. First consider the simplest case of ions with charge q in a uniform electric field in the x direction, $\boldsymbol{F} = qE\hat{\boldsymbol{x}}$. The Langevin equation becomes $\ddot{x} = -\gamma\dot{x} + R_x/m + qE/m$. Taking the ensemble average and assuming a steady-state situation, $\langle\ddot{x}\rangle = 0$, one obtains $\langle\dot{x}\rangle = qE/m\gamma$. Substituting this average velocity in flux yields $J_x = n\langle\dot{x}\rangle = (nq/m\gamma)E$, which is Ohm's law with the conductivity given by $\sigma = nq/m\gamma = nqD/kT$. These cases demonstrate the equivalence of BD to continuum theories in bulk electrolytes in some limiting situations. There are no simple solutions of the Langevin equation when both potential and concentration gradients are present in the system. Nevertheless, the general equivalence of the two approaches in bulk solutions can be established by comparing solutions of PNP equations with BD simulation results. The upshot is that there is not much point in using BD for simulation of bulk electrolytes or bulk-like systems (e.g. channels where ion–channel interaction is ignored). The continuum theories will do the same job at a fraction of the computational cost. BD becomes an indispensable tool only when one needs to model ions' interactions with boundaries accurately, as in the case of ion channels.

BD algorithms for ion channels. During permeation, forces acting on ions in a channel change rapidly with space and time. In order to model ion permeation correctly, both calculation of $\boldsymbol{F}$ and its implementation in the Langevin equation via numerical integration must be done accurately. We tackle the latter issue first and describe a third-order algorithm which has general validity regardless of the time step used (van Gunsteren and Berendsen 1982). Again, we consider (24) in the x direction (identical results follow in the other directions), $\ddot{x} + \gamma\dot{x} = (R + F)/m$. The ion and coordinate labels are suppressed here for convenience. Using $\ddot{x} + \gamma\dot{x} = \mathrm{e}^{-\gamma t}\frac{\mathrm{d}}{\mathrm{d}t}(\dot{x}\mathrm{e}^{\gamma t})$, this equation can be integrated from an initial time t_n to t, giving

$$\dot{x}(t)\,\mathrm{e}^{\gamma t} - \dot{x}(t_n)\,\mathrm{e}^{\gamma t_n} = \frac{1}{m}\int_{t_n}^{t}[R(t') + F(t')]\,\mathrm{e}^{\gamma t'}\,\mathrm{d}t'. \tag{30}$$

Here the integral over the random force follows directly from its stochastic properties. Assumption of a constant systematic force during a time interval Δt simplifies the solution of (30) somewhat. However, such an algorithm, second order in Δt, is valid only for $\Delta t \ll \gamma^{-1}$. This restriction is avoided by going to the third order, which requires the knowledge of the

next order term in the Taylor expansion of the systematic force, $F(t) = F(t_n) + \dot{F}(t_n)(t - t_n)$. Performing the integrations in (30) with this force gives

$$\dot{x}(t) = \dot{x}(t_n)\,\mathrm{e}^{-\gamma(t-t_n)} + \frac{F(t_n)}{m\gamma}\left(1 - \mathrm{e}^{-\gamma(t-t_n)}\right) + \frac{\dot{F}(t_n)}{m\gamma^2}\left(\gamma(t - t_n) - 1 + \mathrm{e}^{-\gamma(t-t_n)}\right) + \frac{\mathrm{e}^{-\gamma t}}{m}\int_{t_n}^{t} R(t')\,\mathrm{e}^{\gamma t'}\,\mathrm{d}t'. \tag{31}$$

The position after a time step Δt is found by integrating (31) from t_n to $t_{n+1} = t_n + \Delta t$. Integration of all the terms in (31) are straightforward except the last one which can be done by parts using $\mathrm{d}u = \mathrm{e}^{-\gamma t}$ and v as the integral of R_x

$$\int_{t_n}^{t_{n+1}} \mathrm{e}^{-\gamma t}\int_{t_n}^{t} R_x(t')\,\mathrm{e}^{\gamma t'}\,\mathrm{d}t' = \frac{1}{\gamma}\int_{t_n}^{t_{n+1}}\left[1 - \mathrm{e}^{\gamma(t-t_n-\Delta t)}\right]R_x(t)\,\mathrm{d}t \equiv X_n(\Delta t), \tag{32}$$

where the random variable $X_n(\Delta t)$ has the same stochastic properties as $R_x(t)$ (see van Gunsteren and Berendsen (1982) for details of its implementation in the BD algorithm). With this result, the position at time t_{n+1} becomes

$$x(t_{n+1}) = x(t_n) + \frac{\dot{x}(t_n)}{\gamma}(1 - \mathrm{e}^{-\tau}) + \frac{F(t_n)}{m\gamma^2}(\tau - 1 + \mathrm{e}^{-\tau}) + \frac{\dot{F}(t_n)}{m\gamma^3}\left(1 - \tau + \tau^2/2 - \mathrm{e}^{-\tau}\right) + X_n(\Delta t). \tag{33}$$

Here $\tau = \gamma\Delta t$ is a dimensionless parameter that signifies a ballistic regime when $\tau \ll 1$ and a diffusive one when $\tau \gg 1$. In these two limits, equation (33) simplifies to

$$\begin{aligned} x(t_{n+1}) &= x(t_n) + \dot{x}(t_n)\Delta t + \frac{F(t_n)}{m}\frac{\Delta t^2}{2} + \frac{\dot{F}(t_n)}{m}\frac{\Delta t^3}{3!}, && \Delta t \ll \gamma^{-1}, \\ x(t_{n+1}) &= x(t_n) + \frac{\dot{x}(t_n)}{\gamma} + \frac{F(t_n)}{m\gamma}\Delta t + \frac{\dot{F}(t_n)}{m\gamma^2}\frac{\Delta t^2}{2} + X_n(\Delta t), && \Delta t \gg \gamma^{-1}. \end{aligned} \tag{34}$$

In the ballistic limit, friction is ignored and the result is in accordance with the numerical integration of Newton's equation of motion as employed in MD simulations (the Verlet algorithm, Verlet (1967)). Of more relevance here is the diffusive limit, which can be further simplified by neglecting the smaller velocity and $\dot{F}(t_n)$ terms. The resulting expression then corresponds to the solution of the diffusive Langevin equation where the inertial term $m\ddot{x}$ is omitted from (24). Because of its simplicity, this form is quite popular in the literature. However, its applicability to ion channels is limited by the condition $\Delta t \gg \gamma^{-1}$, which requires use of rather large time steps (i.e. $\Delta t \gg 30$ fs). This is as opposed to the rapidly changing forces inside a channel that demand use of much smaller time steps than 30 fs.

In practical applications, the velocity term is eliminated from $x(t_{n+1})$ by adding $\mathrm{e}^{-\tau}x(t_{n-1})$ to equation (33)

$$x(t_{n+1}) = x(t_n)(1 + \mathrm{e}^{-\tau}) - x(t_{n-1})\,\mathrm{e}^{-\tau} + \frac{F(t_n)}{m\gamma^2}\tau(1 - \mathrm{e}^{-\tau}) + \frac{\dot{F}(t_n)}{m\gamma^3}\tau\left(\tau(1 + \mathrm{e}^{-\tau})/2 - 1 + \mathrm{e}^{-\tau}\right) + X_n(\Delta t) + X_n(-\Delta t)\,\mathrm{e}^{-\tau}. \tag{35}$$

A similar expression is obtained for the velocity by subtracting $x(t_{n-1})$ from (33)

$$\dot{x}(t_n) = \frac{2\gamma}{\sinh\tau}\left[x(t_{n+1}) - x(t_{n-1}) + 2\left(\frac{F(t_n)}{m\gamma^2} - \frac{\dot{F}(t_n)}{m\gamma^3}\right)(\sinh\tau - \tau) - X_n(\Delta t) + X_n(-\Delta t)\right]. \tag{36}$$

Equations (35) and (36) (and similar ones for y and z) provide the basic input for the third-order algorithm used in BD simulations. At each time step, the calculated values of F and $\dot{F}$ and the sampled value of X_n are fed into (35) and (36) to determine the new positions and velocities of ions in the system. This process is repeated until a statistically meaningful trajectory data set is generated so that properties of interest such as average concentration, potential and current can be calculated with confidence.

Calculation of forces. We next discuss systematic forces and how they can be calculated both accurately and fast enough to enable long-time BD simulations. For convenience, we separate the electric and short-range forces acting on ions as $\boldsymbol{F}_i = q_i \boldsymbol{E}_i + \boldsymbol{F}_{si}$. The total electric field at the position of the ion i can be determined fairly accurately from numerical solution of Poisson's equation (section 2). However, as stressed earlier, the fact that this process needs to be repeated millions of times during a typical BD simulation creates a computational bottleneck. One way to overcome this problem is to precalculate the electric potential and field on a grid of points and store these values in a set of tables (Hoyles *et al* 1998a). During simulations, the potential and field at desired points are determined by interpolating between the table entries. For calculational convenience, the total potential φ_i experienced by an ion i is broken into four pieces using the superposition principle

$$\varphi_i = \varphi_{X,i} + \varphi_{S,i} + \sum_{j \neq i} (\varphi_{C,ij} + \varphi_{R,ij}), \tag{37}$$

where the sum over j runs over all the ions in the system, and the four terms refer to

(i) $\varphi_{X,i}$ is the external potential due to the applied field, fixed charges in the protein, and the surface charges induced by these on the channel boundary. Because it is independent of ions, φ_X does not change during simulations. Poisson's equation is solved in the absence of ions and the results at the grid points are stored in a 3D table.

(ii) $\varphi_{S,i}$ is the self-potential due to the charges induced by the ion i itself on the boundary. Poisson's equation is solved for a single ion with the applied field and fixed charges switched off. The ion is moved through the grid points and the calculated self-potentials are stored in a 3D table (2D if the channel boundary is axially symmetric).

(iii) $\varphi_{C,ij}$ is the Coulomb potential due to the ion j. It is calculated directly from the Coulomb law.

(iv) $\varphi_{R,ij}$ is the reaction potential due to the charges induced by the ion j. This is similar to case (ii) except that a second ion is moved through all the grid points while the first one is held at one point. Because the solution of Poisson's equation contains the Coulomb and self-potentials at the position i, these need to be subtracted to obtain $\varphi_{R,ij}$. The results are stored in a 6D table (5D if the boundary is axially symmetric).

An identical procedure is used to store the three components of the electric field in three sets of tables. The accuracy of this method clearly depends on the choice of grid points. For example, use of a rectangular grid with a uniform spacing would certainly defeat the purpose because the electric field changes rapidly in narrow parts of a channel but less so in wider parts and hardly at all in reservoirs. This problem is avoided by using generalized coordinates, which allows variations in grid spacing as necessary. Tests indicate that, with this method, forces acting on ions in channels can be calculated very accurately (Hoyles *et al* 1998a).

The short-range forces among ions or between an ion and protein or lipid wall are also Coulombic in nature but arise from quantum mechanical effects. When the electronic orbitals of two atoms overlap, a very steep repulsive force occurs due to the Pauli exclusion principle. From the tail of electronic wavefunctions, one expects this repulsive interaction to have an exponential form $e^{-\alpha r}$, where r is the distance between the two atoms. But power laws such

as r^{-12} are preferred in practice because they are more convenient computationally and lead to similar results. At larger separations, the induced dipole–dipole interaction leads to a weak r^{-6} attraction between two atoms (dispersion or van der Waals interactions). In MD simulations of liquids, these two effects are commonly combined in a 12–6 Lennard-Jones (LJ) potential

$$U_{\mathrm{LJ}} = 4\epsilon\big[(\sigma/r)^{12} - (\sigma/r)^{6}\big], \tag{38}$$

where ϵ is the depth of the potential at the minimum ($r_{\min} = 2^{1/6}\sigma$), and σ is where it vanishes. Clearly the raw LJ interaction between two ions will be greatly modified in the presence of solvent molecules, and cannot be employed in BD simulations in the form it is used in MD. When the LJ potential is averaged over many atoms, the weak attractive part is typically washed out and the strong repulsive part acquires an r^{-9} dependence as a result of 3D integration. More importantly, MD simulations show that the hydration forces add further structure to the ion–ion interaction in the form of damped oscillations (Guàrdia *et al* 1991a, 1991b). The potential of mean force between two ions obtained from such MD simulations can be approximately represented by (Moy *et al* 2000)

$$U_{\mathrm{ii}}(r) = u_0\big\{(R_{\mathrm{c}}/r)^9 - \exp[(R-r)/a_{\mathrm{e}}]\cos[2\pi(R-r)/a_{\mathrm{w}}]\big\}. \tag{39}$$

Here u_0 is the overall strength of the potential and R_{c} is the contact distance for anion–cation pairs, which is pushed further apart (by 1.6 Å) for like ions. The second term in (39) describes the damped oscillations with $R \sim R_{\mathrm{c}}$ and $a_{\mathrm{e}} = 1$ Å. Since they are caused by water molecules, the oscillation length is given by the water diameter $a_{\mathrm{w}} = 2.76$ Å. The values of other parameters are determined from fits to the potentials of mean force (Corry *et al* 2001). The advantage of using the ion pair potentials (39) in BD simulations is that they lead to a more realistic distribution of ions as compared with the simple hard-core or repulsive r^{-9} potentials. As will be seen in the next section, this is an important consideration in modelling of multi-ion channels.

The main function of the ion–wall interaction is to keep the ions in the system. Due to the repulsive image forces, ions usually stay well away from the boundaries. However, on occasion an ion can stray outside due to a large fluctuation in the random force. This is prevented by using an r^{-9} repulsive potential U_{iw} at the walls, where r is the distance of the ion from the boundary. The total short-range force acting on an ion is obtained from the gradient, $\boldsymbol{F}_{\mathrm{s}} = -\nabla(U_{\mathrm{ii}} + U_{\mathrm{iw}})$.

Reservoirs and boundary conditions. To complete the simulation system, electrolyte-filled reservoirs are attached on either side of the lipid–channel complex. This is just a book-keeping device to facilitate tracking of the ions in the system. Otherwise the electrolyte solution is assumed to continue beyond the reservoirs. The shape of the reservoirs is arbitrary (for example, it could be rectangular, spherical or cylindrical), but their dimensions need to be chosen carefully. If the reservoirs are too large, time is wasted on simulating the motion of ions that are far away from the channel, and therefore have no influence on the permeation dynamics. Conversely, if the reservoir size is too small, ion–channel interactions may not be modelled accurately. Recalling from section 2.2 that an ion's electric field is totally screened out at about 4 Debye lengths, one can safely ignore the ions beyond that distance from the channel mouth. Thus, for physiological concentrations (0.15 M), the optimal radius or length for the reservoirs is ∼30 Å.

Once an optimal size is chosen for the reservoirs, handling of their boundaries should not be a significant issue. Since the physics is in the ion–channel interactions, not in the reservoir boundaries, it is desirable to use the simplest method possible. Unfortunately, because this is a delicate issue in MD simulations due to the long-range Coulomb forces in vacuum (see the textbooks on MD quoted in the next section), the same is assumed to be the case

for BD simulations, resulting in use of unnecessarily complicated boundaries. In fact, in BD simulations, dielectric and Debye screening ensures that one need not worry about what happens beyond the reservoir boundaries. The simplest method is to confine the ions within the simulation system by elastically scattering them off the reservoir boundaries. In this way one maintains the average concentrations in the baths at the desired values at all times. In reality, ions would move in and out of the reservoir leading to fluctuations in average concentrations, which in turn may cause fluctuations in current. Recently, Im *et al* (2000) introduced a grand canonical Monte Carlo method that takes such fluctuations in concentrations into account. This method is useful if one is interested in understanding the fluctuations in observed channel current, which is a rather ambitious goal for the relatively crude BD simulations. For the more modest aim of interpreting the average value of channel current, keeping the reservoir concentrations constant at their average values should be quite adequate. In any case, the important quantity to consider is the number of ions in the vicinity of the channel, and this has been shown to fluctuate according to the binomial distribution regardless of whether one fixes the total number of ions or allows it to fluctuate according to the grand canonical distribution (Corry *et al* 2001b). Another purported advantage of this method is that it allows non-integer values for the average number of ions that arise when the reservoir concentrations and volume are chosen arbitrarily. Of course, this is not really a problem in the simpler method since for a given concentration, the volume can be slightly adjusted to make the number of ions integer.

A related point is how to maintain the specified concentrations in the reservoirs when a current flows through the channel. The simplest method is to apply a stochastic boundary, namely, when an ion crosses the channel, say from left to right, an ion of the same species is transplanted from the right reservoir to the left, thereby completing the circuit. Disturbance of the system due to this sudden relocation of an ion can be minimized by choosing the ion nearest to the boundary and putting it next to the boundary on the other side. To give an example, the effect of this procedure on another ion in the channel would be a change in the force acting on it by a fraction of pN, which is an order of magnitude smaller than the force due to a membrane potential of 0.1 V (2 pN) and completely negligible compared with the random and frictional forces (1–2 nN).

A final topic to be considered is the implementation of the membrane potential in BD simulations. Again, this is an elementary issue and should be straightforward to implement. Unfortunately, it is often misunderstood in channel studies, so it is worthwhile to give a brief account of the physics involved to clarify any confusion. When a voltage difference is applied across the membrane via electrodes at macroscopic distances, anions and cations move in opposite directions until the electric field in the solution vanishes. This results in an excess cloud of anions on one side of the membrane and cations on the other. Average behaviour of these excess charges can be approximately represented by uniformly charged planes, which generate a uniform electric field across the membrane. Thus the easiest way to implement the membrane potential is to simply apply a uniform electric field in the system. Note that this is only one part of the total field and this field itself is modified by the dielectric boundary inside the channel. The actual potential difference is determined from the solution of Poisson's equation or, if one insists on a more accurate measurement, from the average potentials at the centre of the reservoirs calculated during the BD simulations. An alternative method for applying the membrane potential is to fix their values at the reservoir boundaries. Strictly speaking, the potentials are fixed at the electrodes far away, and the regular surfaces chosen for boundaries will not be equipotential surfaces in reality. Nevertheless, in practice, the difference between the two methods is negligible—when the reservoir size is chosen as prescribed above, the potential values at the boundaries differ by at most a few per cent. A similar result is obtained from a comparison of potentials using the method of Im *et al* (2000) (Corry *et al* 2001b). But more importantly, these differences between various methods near the boundary

are quickly dissipated once one moves away from it, and one can hardly distinguish between their predictions for concentration or potential in or near the channel.

Limitations of BD. The treatment of water as a continuum is both a strength and a weakness of the BD approach. While it reduces the simulation time by many orders of magnitude as compared with MD, thus enabling calculation of conductance, it also ignores the differences between hydration energies of ions, which is essential for understanding the selectivity sequences among monovalent cations. We stress that this limitation applies only when selectivity is based on size rather than charge of ions. Otherwise, selectivity between anions and cations or mono- and divalent ions can still be understood within the BD framework. A second problem is the diffusion coefficient of ions in channels. The bulk values of D are well known but it is almost certain that they will be suppressed in a narrow pore. As discussed in section 2.3, there is the question of validity of continuum electrostatics in channels and, assuming it is valid, the effective value of the dielectric constant one should use. Finally, implicit in the continuum formalism is the assumption of rigid channel boundaries. Channel proteins are certainly not static, but the crucial question is whether there are any correlations between their motion and permeating ions. If such correlations are negligible, use of rigid boundaries reflecting the average position of protein walls would be well justified. Finally, because water is treated as a continuum, the relative distance between ions in a single-filing channel is not constrained by the water molecules that separate the ions. This problem is addressed to some degree by using the ion–ion interaction potentials determined from the MD potential of mean force (39), which maintains the correct distance between the ions when they are separated by a few water molecules. In cases where ion separation is larger (e.g. GA), this effect of the water molecules needs to be taken into account explicitly. In order to address these questions, one needs to go to the next level in hierarchy and appeal to MD simulations.

In principle, it is possible to by-pass all these problems and make BD quite rigorous by determining the local diffusion coefficient and the average forces acting on ions from MD simulations. After direct MD simulations, this would offer the most rigorous method for determination of channel conductance. However, the computations involved are very heavy (especially for multi-ion channels), and no attempt has been made in this direction so far. In the meantime, MD simulations can be used to complement those of BD, for example, to explain selectivity among ions with the same charge, determine appropriate values of D for ions in channels, study validity of continuum electrostatics, and attempt to determine an effective ε value for channel water.

3.3. Molecular dynamics

Parallel to the increase in computer power, applications of MD simulations to problems in physics, chemistry and biology have been growing at a phenomenal rate. The availability of several user-friendly packages specifically designed for simulation of biomolecular systems, such as AMBER (Weiner *et al* 1984), CHARMM (Brooks *et al* 1983) and GROMOS (Hermans *et al* 1984), has been instrumental in bringing the MD method to the masses in biophysics and biochemistry. Early applications of MD to ion channels were focused on the GA channel because of its known structure (see section 4.1 for details). From the mid-1990s on, other synthetic channels and schematic pores were studied using MD. The appearance of the KcsA potassium channel structure (Doyle *et al* 1998) finally led to an explosion in applications of MD that continues unabated (see section 4.2 for details). There is also a negative side to this proliferation, as uncritical usage of MD could hinder progress rather than helping it. In this respect, there are some parallels between the use of continuum theories and MD in ion channels—in both cases models developed for bulk solutions are applied to channels without

establishing their validity in the new environment. In order to point out some potential problems with such straightforward usage of the standard MD packages in channels, we first consider the fundamental formalism at the quantum mechanical level. This is followed by a critical evaluation of classical and *ab initio* MD, and a discussion of uses of MD methods in channels. While MD simulations are conceptually simple (solving Newton's equation of motion), there are many technical issues related to the treatment of boundaries and extraction of physical quantities from statistical analysis of trajectory data. These topics are discussed in great detail in several excellent textbooks (Allen and Tildesley 1987, Rapaport 1995, Frenkel and Smit 1996), and the interested reader is referred to them. Here we go straight to the heart of the matter: that is, the force fields employed in MD.

Basic formalism. At a fundamental level, a system of interacting atoms is described by the many-body Schrödinger equation

$$(H_{\mathrm{n}} + H_{\mathrm{e}} + U_{\mathrm{ne}})\psi(\{\boldsymbol{R}_i, \boldsymbol{r}_\alpha\}) = E\psi(\{\boldsymbol{R}_i, \boldsymbol{r}_\alpha\}), \tag{40}$$

where the indices i and α run over the nuclei (or ions with closed electronic shells) and the electrons in the system, ψ is a properly antisymmetrized total wavefunction and E is the corresponding energy eigenvalue. The first two terms in the Hamiltonian describe the nuclear and electronic parts and the last one the Coulomb interaction between them

$$\begin{aligned} H_{\mathrm{n}} &= -\sum_i \frac{\hbar^2}{2M_i}\nabla_i^2 + \sum_{i>j}\frac{z_i z_j e^2}{|\boldsymbol{R}_i - \boldsymbol{R}_j|} \\ H_{\mathrm{e}} &= -\sum_\alpha \frac{\hbar^2}{2m}\nabla_\alpha^2 + \sum_{\alpha>\beta}\frac{e^2}{|\boldsymbol{r}_\alpha - \boldsymbol{r}_\beta|} \\ U_{\mathrm{ne}} &= -\sum_{i,\alpha}\frac{z_i e^2}{|\boldsymbol{R}_i - \boldsymbol{r}_\alpha|}. \end{aligned} \tag{41}$$

Here M_i refers to the mass of nuclei and m to that of electrons. This hopelessly complicated equation is brought into some relief by exploiting the fact that nuclei, being much heavier than electrons, move much more slowly, and therefore their motion can be decoupled from those of electrons: that is, $\psi(\{\boldsymbol{R}_i, \boldsymbol{r}_\alpha\}) = \psi_{\mathrm{n}}(\{\boldsymbol{R}_i\})\psi_{\mathrm{e}}(\{\boldsymbol{R}_i, \boldsymbol{r}_\alpha\})$. Using this product wavefunction in (40), the electronic part can be formally written as

$$(H_{\mathrm{e}} + U_{\mathrm{ne}})\psi_{\mathrm{e}}(\{\boldsymbol{R}_i, \boldsymbol{r}_\alpha\}) = E_{\mathrm{e}}(\{\boldsymbol{R}_i\})\psi_{\mathrm{e}}(\{\boldsymbol{R}_i, \boldsymbol{r}_\alpha\}). \tag{42}$$

In the adiabatic or Born–Oppenheimer approximation, the two terms of order $(m/M_i)^{1/2}$ and m/M_i that arise from the action of H_{n} on ψ_{e} are neglected, so that the nuclear part becomes

$$[H_{\mathrm{n}} + E_{\mathrm{e}}(\{\boldsymbol{R}_i\})]\psi_{\mathrm{n}}(\{\boldsymbol{R}_i\}) = E\psi_{\mathrm{n}}(\{\boldsymbol{R}_i\}). \tag{43}$$

Apart from very simple systems, solution of equations (42) and (43) is still very formidable, and a second approximation is invoked at this stage by treating the nuclear motion classically. For example, the ground state of the system (zero temperature) is determined by minimizing the potential energy surface for nuclei (or ions)

$$U(\{\boldsymbol{R}_i\}) = \sum_{i>j}\frac{z_i z_j e^2}{|\boldsymbol{R}_i - \boldsymbol{R}_j|} + E_{\mathrm{e}}(\{\boldsymbol{R}_i\}), \tag{44}$$

with respect to the coordinates $\{\boldsymbol{R}_i\}$. Here $E_{\mathrm{e}}(\{\boldsymbol{R}_i\})$ is taken from the ground-state solution of (42). At finite temperatures, assuming that electrons remain in their ground state, one can use the potential function (44) in Newton's equation of motion

$$M_i\ddot{\boldsymbol{R}}_i = -\nabla_i U(\{\boldsymbol{R}_i\}), \tag{45}$$

to trace the motion of individual nuclei. Together with equations (42) and (44), equation (45) forms the basis of *ab initio* MD simulations. The formalism reduces to classical MD when the electronic degrees of freedom are ignored and a fixed functional form is assumed for the potential in (45) from the outset.

The intermolecular potential in equation (44) is seen to consist of a classical electrostatic and a quantum mechanical electronic part. In a perturbation analysis, the electronic interaction between two molecules can be separated into three further terms: polarization, dispersion and exchange repulsion. The last two terms are usually approximated using the 12–6 LJ potentials in classical simulations as discussed in the BD section. The polarization interaction can also be given a classical description by assigning polarizabilities to individual atoms or molecules. However, it is often neglected in applications of MD to ion channels because most MD packages employ nonpolarizable force fields. The importance of the polarization effects in MD studies of ion permeation in channels is one of the central themes of this review and is discussed in more detail below.

The adiabatic and classical approximations in the above formalism are expected to work well for heavy atoms but not for the lighter ones, especially hydrogen. Note that implicit in use of (42) in the calculation of E_e is the assumption that electrons remain in their ground state at finite ($\sim$room) temperatures. Also at finite temperatures, atomic collisions can induce electronic transitions leading to excitations from the ground state. Such non-adiabatic effects are expected to play an important role in dynamic situations (e.g. chemical reactions where bonds are formed or broken), but not in equilibrium (or near equilibrium) where they are thought to be negligible (Tuckerman *et al* 1996). Therefore, we will not go into refinements of *ab initio* MD here. That also means excluding discussion of the interesting case of proton permeation in channels. Because a proton is light and its transfer involves the making and breaking of hydrogen bonds, it has to be treated quantum mechanically (Sagnella *et al* 1996, Geissler *et al* 2001).

The usual computational bottleneck in all simulation work arises from the fact that forces need to be re-evaluated at each time step. This problem is much worse in the case of *ab initio* MD because solution of the many-body Schrödinger equation (42) is an extremely time consuming process. Comparison of the number of water molecules that can be handled and simulation times in *ab initio* MD ($\sim 10^2$ molecules for picoseconds) with those in classical MD ($\sim 10^5$ molecules for nanoseconds) gives an indication of the magnitude of the problem. Note that a water molecule is represented by three ions and eight electrons in the former and by three atoms in the latter, so the severe limitation in simulation size and time in *ab initio* MD is due to going from classical to quantum dynamics rather than the extra particles involved.

Classical MD. A purely classical description of a system can be obtained by replacing the *ab initio* potential energy (44) with a phenomenological one, which can be expanded in many-body terms as

$$U(\{\boldsymbol{R}_i\}) = \sum_{i>j} U_2(\boldsymbol{R}_i, \boldsymbol{R}_j) + \sum_{i>j>k} U_3(\boldsymbol{R}_i, \boldsymbol{R}_j, \boldsymbol{R}_k) + \cdots. \tag{46}$$

The usual experience with many-body systems is that the two-body part dominates the total energy, and contributions from the higher-order terms rapidly diminish with increasing order. Thus a reasonable method to construct the many-body potential is to start with the dimer system and determine U_2 first, and then proceed with the trimer, tetramer, etc, subtracting at each step contributions from the lower-order energies to obtain the corresponding many-body interaction. For water, the main substance of interest in MD simulations, this approach was initiated by Clementi and collaborators (Matsuoka *et al* 1976). Despite the continuing efforts of several groups for over two decades, a water potential that successfully simulates its liquid

Table 2. Parameters of water models commonly used in MD simulations. The last two columns give the dipole moments μ and dielectric constants ε (from Höchtl *et al* (1998)). The experimental value of μ in the gas phase is 1.86 D (Clough *et al* 1973).

Model	r_{OH} (Å)	θ_{HOH}	q_H (e)	ϵ (kT)	σ (Å)	μ (D)	ε
SPC	1.0	109.5°	0.410	0.262	3.166	2.27	65 ± 5
TIP3P	0.957	104.5°	0.417	0.257	3.151	2.35	97 ± 7

properties has yet to be constructed (see Wallqvist and Mountain (1999) for a review of water models). As in many other strongly interacting systems, it is very difficult to describe the collective or co-operative effects in water by simply summing up the many-body terms.

The alternative is to truncate the many-body potential energy (44) at the two-body level and try to incorporate the effects of the higher-order terms in the parametrization of U_2 within a mean field approximation. This approach has been widely adopted in practical applications and forms the basis of all the current MD simulation packages. Since an accurate description of water is a key ingredient in their success, we describe the water models used in these packages. The two models that have become the industry standard are SPC (simple point charge, Berendsen *et al* (1981)) and TIP3P (transferable intermolecular potential with three points, Jorgensen *et al* (1983)). Both are rigid, three-site models that try to capture the tetrahedral coordination of water molecules in liquid using the known H_2O geometry with partial charges at the O and H sites. Thus, the basic parameters are the O–H distance r_{OH}, the H–O–H angle θ_{HOH} and the partial charges on hydrogens q_H ($q_O = -2q_H$ from electroneutrality). In addition, the dispersion and repulsive short-range interactions between the oxygen sites are represented by a 12–6 LJ potential (38). The parameters of the two models (table 2) are quite similar as are their overall performance in predicting water properties. Note that θ_{HOH} in SPC corresponds to the ideal tetrahedral angle whereas θ_{HOH} (and r_{OH}) in TIP3P are taken from the experimental values of the water monomer. This apparently small difference in θ_{HOH} is responsible for the 50% difference in dielectric constants, which would be hard to explain on the basis of the 3% difference in the dipole moments alone. Höchtl *et al* (1998) have shown that θ_{HOH} is by far the most critical determinant of ε and the tetrahedral choice in SPC actually minimizes it. Changing the SPC angle by either $-5°$ or $+5°$ leads to $\sim$50% increase in ε values, despite a reduction in μ in the latter case. This result should have important ramifications in the design of new water models because the dipole moment was long thought to be the crucial parameter in determining the dielectric constant (Sprik 1991).

Both water models have improved versions that give a better description of bulk properties such as radial distribution functions and diffusion coefficients. SPC was extended to SPC/E (Berendsen *et al* 1987) by including the polarization energy in the fitting procedure, which yielded slightly higher charges, $q_H = 04238e$. A four-site version of TIP3P, called TIP4P (Jorgensen *et al* 1983), was constructed by moving the charge on the oxygen site by 0.15 Å along the H–O–H bisector and increasing the charges to $q_H = 0.52e$. Despite the improvements, the original versions continue to be employed in biomolecular simulations because, as stressed by Tieleman *et al* (1997), SPC has a better chemical potential in mixed systems and therefore it is more suitable for such applications. This brings us back to the missing term in the SPC and TIP3P force fields: namely, the polarization interaction. To put this issue into a proper perspective, we note that water molecules have a relatively large polarizability ($\alpha = 1.444$ Å^3), and the polarization contribution to the total energy of a water molecule, estimated from quantum chemical calculations, is about 20% in a dimer rising to 44% in liquid water (Engkvist *et al* 2000). These are significant figures and one would not expect the models to work at all if they completely ignored polarization contribution to the energy. Indeed, the

effects of polarization are absorbed in the other terms in SPC and TIP3P by ensuring that the experimental energy in liquid is reproduced by the models. That is why, for example, the μ values quoted in table 2 are substantially larger than the experimental one. This approximation seems to work well in simulations of pure water, but problems will arise in dealing with mixed systems, especially when it involves transport of ions from one environment to another with very different polarization characteristics.

The solution to this dilemma is to include the polarization interaction explicitly in the force fields. Despite the computational costs involved, there have been serious efforts in this direction during the last decade (for reviews, see Halgren and Damm (2001), Wallqvist and Mountain (1999)). Conceptually the simplest method is to introduce point dipole polarizabilities at the atomic sites so that an electric field $\boldsymbol{E}_i$ at a site i induces a dipole moment $\delta\vec{\mu}_i = \alpha_i \boldsymbol{E}_i$, assuming an isotropic polarizability of α_i (Barnes *et al* 1979, Rullmann and van Duijnen 1988, Dang 1992, Dang and Chang 1997). Since the electric field arises from both the permanent partial charges and the induced dipoles on other sites, the induced dipole moment can be written as

$$\delta\vec{\mu}_i = \frac{\alpha_i}{4\pi\varepsilon_0} \sum_{j\neq i} \left[\frac{q_j \hat{\boldsymbol{r}}_{ij}}{r_{ij}^2} + \frac{1}{r_{ij}^3}(3\hat{\boldsymbol{r}}_{ij}\hat{\boldsymbol{r}}_{ij} \cdot \delta\vec{\mu}_j - \delta\vec{\mu}_j) \right], \tag{47}$$

where $\boldsymbol{r}_{ij} = \boldsymbol{r}_j - \boldsymbol{r}_i$ and $\hat{\boldsymbol{r}}_{ij}$ denotes the unit vector. Equation (47) displays the genuinely many-body nature of the polarization interaction—it cannot be reduced to pairwise additive terms as in Coulomb and LJ potentials. Thus to calculate the induction forces and energies, one needs to solve the coupled system of equations in (47) by matrix inversion or iteration at each time step. This increases the simulation time several-fold, which may explain the prevailing reluctance to including the polarization effects in MD studies. A computationally less demanding method to describe polarizability is to allow fluctuations in the partial charges in response to the environment (Sprik and Klein 1988, Rick *et al* 1994). However, polarization is confined to the molecular plane in this method, so it may require supplementing with point dipoles for molecules with isotropic polarizabilities (e.g. water).

The general conclusion from the decade-long studies of bulk water and electrolyte solutions with polarizable models is that they provide little (if any) improvement over the standard nonpolarizable models (Halgren and Damm 2001, Koneshan *et al* 2001). In part, this reflects the success of the mean field treatment of polarization effects in the standard models. Another reason for this somewhat disappointing result is perhaps the way that a majority of the polarizable models are constructed by 'grafting' point dipoles on one of the standard models with a minimal adjustment of partial charges. Constructing a successful water model by 'guessing' the parameters is said to be an art form. It would be desirable to reduce it to a science by determining the force field parameters directly from the *ab initio* calculations (Wallqvist and Karlström 1989, Engkvist *et al* 2000, Guillot and Guissani 2001). This is even more pressing in mixed systems, where there is an emerging consensus that polarization effects should be taken into account properly.

Ab initio MD. Quantum chemical methods have long been used to determine the potential energy surfaces in atomic and molecular systems. The main approach is to solve the Schrödinger equation using the Hartree–Fock theory and its various improvements (Pople 1999). Because the basis set for the electronic wavefunction increases exponentially with the number of atoms, application of these methods is limited to relatively small systems (currently about ten atoms). A second method, called density functional theory (DFT) (Kohn 1999), has come into prominence in recent years because it can handle much larger systems (currently 10^2–10^3 atoms). In DFT one dispenses with the electronic wavefunction and deals directly

with the electron density distribution. As a result, size dependence becomes a power law, much less limiting than an exponential. In a nutshell, the ground-state density of electrons is given by

$$n(\boldsymbol{r}) = \langle \psi_{\mathrm{e}} | \sum_{\alpha} \delta(\boldsymbol{r} - \boldsymbol{r}_{\alpha}) | \psi_{\mathrm{e}} \rangle, \tag{48}$$

where ψ_{e} is the electronic wavefunction introduced in equation (42) and we have used the Dirac notation for compactness. Various expectation values in the ground-state energy (42)

$$E_{\mathrm{e}} = \langle \psi_{\mathrm{e}} | H_{\mathrm{e}} + U_{\mathrm{ne}} | \psi_{\mathrm{e}} \rangle \tag{49}$$

are expressed as functionals of the density (48). For example, the interaction between the ions and electrons becomes

$$\begin{aligned} \langle U_{\mathrm{ne}} \rangle &= \langle \psi_{\mathrm{e}} | \int \sum_{i,\alpha} \frac{-z_i e^2}{|\boldsymbol{R}_i - \boldsymbol{r}|} \delta(\boldsymbol{r} - \boldsymbol{r}_{\alpha}) \, \mathrm{d}\boldsymbol{r} \, | \psi_{\mathrm{e}} \rangle, \\ &= \int \sum_{i} \frac{-z_i e^2}{|\boldsymbol{R}_i - \boldsymbol{r}|} n(\boldsymbol{r}) \, \mathrm{d}\boldsymbol{r}. \end{aligned} \tag{50}$$

Similarly the electronic part is written as

$$\langle H_{\mathrm{e}} \rangle = T_{\mathrm{s}}[n(\boldsymbol{r})] + \frac{e^2}{2} \int \frac{n(\boldsymbol{r}) n(\boldsymbol{r}')}{|\boldsymbol{r} - \boldsymbol{r}'|} \, \mathrm{d}\boldsymbol{r} \, \mathrm{d}\boldsymbol{r}' + E_{\mathrm{xc}}[n(\boldsymbol{r})], \tag{51}$$

where the first term is the kinetic energy of a noninteracting system and the second one is the classical Coulomb energy. The last term represents the exchange correlations that are left out in the second one. Unlike the other terms, there is no simple form for E_{xc}, and practical applications of DFT hinges on finding good approximations for E_{xc}. For more details on DFT and various choices available for E_{xc}, we refer to the textbooks of Parr and Yang (1989) and Dreizler and Gross (1991) and the review articles of Kohn *et al* (1996), Kohn (1999) and Bickelhaupt and Baerends (2000).

A breakthrough in computer simulations was the innovative combination of MD with DFT by Car and Parrinello (1985), turning *ab initio* MD into a powerful computational tool, free from the arbitrary parametrizations of the force fields in classical MD. The electronic part of the intermolecular potential (44) is determined from DFT using equations (49)–(51). Initial applications of *ab initio* MD were concentrated in condensed matter physics, but spread to other areas quite rapidly (see Parrinello (1997) and Tuckerman and Martyna (1999) for reviews). Of particular interest for this review are the hydrogen-bonded systems, of which water is a prime example. An initial *ab initio* study of liquid water with 32 molecules for 1.5 ps (Laasonen *et al* 1993) was followed up using an improved density functional (Sprik *et al* 1996) with 64 molecules for 10 ps (Silvestrelli and Parrinello 1999). These studies have shed much light on the electronic and bonding properties of water molecules in liquid that would be very useful in constructing new water models. For example, the bond length and angle of a water molecule in liquid are found to be larger than the monomer values (but not as large as employed in SPC). A provocative result from Silvestrelli and Parrinello (1999) is the average dipole moment of $\mu \approx 3.0$ D in liquid, which is substantially larger than the commonly accepted value of 2.6 D in the literature (Coulson and Eisenberg 1966). In fact, this value was calculated for ice I_{h}, but it is often misquoted for liquid water, or even sometimes as an experimental value for liquid. Moreover, a recent re-evaluation of μ for ice I_{h} using the same formalism but with more recent experimental input gave $\mu = 3.09$ D (Batista *et al* 1998). These results are significant for polarizable water models because they have often been criticized in the past for predicting $\mu > 2.6$, which is believed to yield a dielectric constant that is much larger than the experimental value. Both the *ab initio* calculation (Silvestrelli and Parrinello 1999) and a

recent polarizable water model with $\mu = 3.09$ D (Guillot and Guissani 2001) give reasonable ε values, demonstrating that the relationship between μ and ε is not as straightforward as assumed to be (see the correlation between θ_{HOH} and ε in table 2). Another example of *ab initio* MD clearing the muddled waters is the recent Compton scattering experiments in ice I_h (Isaacs *et al* 1999), where the observed anisotropies in directional intensities were widely interpreted as proof of partial covalency of the hydrogen bond (Hellemans 1999, Martin and Derewenda 1999). If true, this would have important ramifications for the standard models of water because they describe the hydrogen bonding in purely classical terms with Coulomb and LJ interactions. As *ab initio* MD calculations demonstrate (Romero *et al* 2001), the anisotropies arise, in fact, from the antibonding repulsive interaction between neighbouring water molecules, which is already included in the 12–6 LJ potential.

The next step for the permeation models is the *ab initio* study of solvation dynamics of ions. Such studies have been initiated recently for several ions, some with biological significance: for example, Be^{2+} (Marx *et al* 1997), Li^+ (Lyubartsev *et al* 2001), Na^+ (White *et al* 2000), K^+ (Ramaniah *et al* 1999) and Cl^- (Tobias *et al* 2001). In general, smaller and more highly-charged ions have more intense electric fields in their first hydration shell, and therefore are more likely to require explicit treatment of polarization in the force fields. This suggests a straightforward assessment of polarizability effects by comparing the average dipole moment of a water molecule in the first hydration shell with that in bulk. Any enhancement would signal the breakdown of the classical models that do not allow any change in the μ values. The ion–oxygen radial distribution functions and coordination numbers are the typical quantities extracted from simulations and frequently used in comparisons of the *ab initio* and classical MD. From the above discussion, the Be^{2+} ion is expected to exhibit the largest discrepancy. Indeed, the classical models with pairwise additive potentials have long been known to fail in reproducing the experimentally observed tetrahedral coordination of water molecules in the first hydration shell of Be^{2+} (Probst *et al* 1989). The *ab initio* calculations, on the other hand, have reproduced the tetrahedral structure, as well as predicting an enhancement in the average μ value in the first hydration shell. Differences between the *ab initio* and classical MD results diminish as one goes from Li^+ to Na^+ and K^+, for the last one being rather negligible. It is worth emphasizing that these comparisons are for bulk electrolytes, and do not justify use of classical models with pair potentials in ion channels even if they agree with the *ab initio* results.

Uses of MD methods in channels. The main application of MD in channels involves calculation of free-energy profiles of ions and some other quantities related to permeation (e.g. ordering of water molecules, diffusion coefficients). Calculation of conductance remains a remote possibility for MD at present because the transit time of a single ion for physiological currents (16 ns for 10 pA) is too long to generate sufficient trajectory data for statistical analysis. A few attempts have actually been made in this direction using very high applied potentials: for example, 0.5 V (Suenaga *et al* 1998) and 1.1 V (Crozier *et al* 2001). Given the non-linear variation of both measured and simulated single-channel currents as a function of potential, it is not clear how these results can be extrapolated to the physiological range of $\sim$0.1 V. Most of the MD calculations have been performed using the simulation packages with the standard force fields quoted earlier. In the light of the foregoing discussion of the MD methods, the absolute free energies of ions are not expected to emerge correctly from such calculations, and indeed this has been the general experience from applications to the GA channel. Inaccuracies arising from the force field parametrizations are likely to cancel out when differences in energies are considered. Thus, predictions of selectivity sequences from free-energy perturbation calculations are expected to be more robust as compared with the absolute energies. Local

properties such as diffusion coefficients should also suffer less from the arbitrariness in force fields. As long as the standard force fields are used in studies of ion channels with the above caveats, they will continue to provide useful information about the permeation dynamics.

There is clearly a pressing need to go beyond the standard force fields in channel studies by constructing polarizable models specifically designed for channels using the *ab initio* calculations as a guide. Previous attempts to include polarization effects in MD studies of GA were not very satisfactory. Although Jordan and collaborators have long recognized their significance (Lee and Jordan 1984, Jordan 1990, Duca and Jordan 1997, 1998), the water and protein models they used were too schematic to allow computation of realistic energy profiles. In other studies, the full channel structure with the TIP3P model was used but polarizability was restricted to the protein only (Roux *et al* 1995, Woolf and Roux 1997). The results were actually worse than those obtained with non-polarizable force fields (Roux and Karplus 1993), which underlines the importance of self-consistency in MD simulations. As demonstrated in a follow-up study by Duca and Jordan (1998), partial incorporation of polarizability introduces larger errors than completely neglecting it.

4. Applications to specific channels

In view of the problems with the continuum description of ions in narrow pores, we will restrict ourselves to theories that represent ions as discrete particles: that is, BD and MD. Applications will focus on three channels, GA, KcsA potassium and L-type calcium, because of their known structure (at least in part), biological significance and theoretical interest. Of course, there are many other channels that satisfy some of these criteria. For example, structures of porin and mechanosensitive channels are known but these are fairly large channels (even the continuum models are expected to work reasonably well in them), and therefore not with many interesting properties. Conversely, too little is known about the tertiary structure of most biological channels to allow quantitative modelling (e.g. sodium, chloride, nicotinic acetylcholine receptor, and a host of other ligand-gated channels). We refer to Hille (1992) for a comprehensive discussion of these channels. There are also a number of synthetic channels formed by bundles of α-helices (e.g. alamethicin, influenza M2 transmembrane helix and leucine–serine peptides) that have been intensely studied with MD simulations in recent years (see Tieleman *et al* (2001) for a detailed review).

4.1. Gramicidin A

For a long time, GA was the only ion channel with a known tertiary structure (Urry 1971), and therefore it has been the main focus of theoretical investigations until recently (see Andersen and Koeppe (1992), Busath (1993), Koeppe and Andersen (1996), Wallace (1998) for general reviews and Pullman (1987), Partenskii and Jordan (1992), Roux and Karplus (1994) for theoretical ones). In membranes, the GA peptide forms a cylindrical channel with length 25 Å and radius 2 Å that selectively conducts monovalent cations, binds divalent cations and rejects all anions. Its physiological properties are well known: linear I–V curves and relatively large half-saturation concentrations point to lack of substantial barriers within the channel, and NMR studies indicate well established binding sites near the entrances.

Modelling of the GA channel has evolved from simple electrostatic calculations with rigid dielectric boundaries (Levitt 1978, Jordan 1982) to sophisticated all-atom MD simulations with GA embedded in a lipid bilayer and solvated with water (Woolf and Roux 1994, 1997, Chiu *et al* 1999). A crucial question that needs to be settled from the outset is whether continuum electrostatics can still be employed when the ion–water system is confined to a single file as

dictated by the GA geometry. Doubts have been raised in this regard earlier (Partenskii *et al* 1994) but a definitive demonstration of the failure of continuum electrostatics in the GA channel has been given very recently (Edwards *et al* 2001)—it is shown that regardless of the effective dielectric constant used for channel water, it is not possible to achieve a consistent description of the experimental data on GA. For example, when $\varepsilon_c = 80$ is employed for channel water, the potential profile for monovalent cations is nearly flat so that one could explain neither the binding sites nor the saturation of conductance. Smaller ε_c values lead to progressively larger central barriers but no wells at the entrances, so the channel ceases to conduct with still no binding sites. Lack of binding sites is found for all types of ions, and points to a general failure of continuum electrostatics in GA. An intuitive explanation for this failure is offered by the fact that the dipole moments of water in the channel are found to be well aligned with the central axis in MD simulations whereas polarizability of water drops as $1/r^2$ with distance from the ion in continuum electrostatics. As the current BD methods rely on continuum electrostatics for the calculation of forces, this leaves MD as the method of choice for studying the structure–function relations in the GA channel. Of course, once reliable potentials of mean force for ions in the GA channel are determined from MD simulations, these can be employed in BD to study its conductance properties. In the meantime one can use inverse methods to find the potential of mean force that reproduces the available data when employed in BD simulations. Such an approach has yielded an $8kT$ well at the entrances and a $5kT$ central barrier (with respect to the well) with a diffusion coefficient of 0.05 times the bulk value for potassium ions (Edwards *et al* 2001).

As already mentioned with regard to the polarization effects, there are two main groups that have made substantial contributions to MD studies of the GA channel. The focus of Jordan's group has been to understand the properties of GA using schematic models, hence agreement with experiment is less emphasized, while Roux and collaborators have attempted to reproduce these properties using realistic models. Their main findings are contrasted with experiments below.

(i) *Free-energy profiles.* The calculated barrier heights are too high to allow ion permeation through the GA channel at the observed rates. For example, for Na^+ ion, Jordan (1987) obtains a translocation barrier of $\sim 40kT$ and Roux and Karplus (1993), $\sim 14kT$. Binding site locations at the channel entrance are generally reproduced by these profiles but again the absolute well depths do not appear to be consistent with the experiments.

(ii) *Ion selectivity.* Because the GA peptide has no net charge, its cation selectivity has been attributed to intricate ion–peptide–water interactions in MD studies (Dorman *et al* 1996, Roux 1996). A recent examination of the charge distribution in the peptide shows that their Coulomb interaction with ions alone leads to a sufficiently high barrier for anions (relative to cations) to exclude them from the channel (Edwards *et al* 2001). The selectivity sequences among monovalent cations, calculated from the free energy differences, are in agreement with the experimental sequence $Cs^+ > K^+ > Na^+ > Li^+$: that is, the larger ions with smaller hydration energies conduct better as in bulk electrolytes (Sancho *et al* 1995, Roux *et al* 1995).

(iii) *Coordination of ions.* A common prediction of all MD simulations is that the backbone of the GA peptide is rather flexible with the carbonyl oxygens swinging up to 20°–40° so that four carbonyls and two water molecules provide a bulk-like solvation environment for a cation in the GA channel. In complete contrast, the recent high-resolution NMR studies of cation transport in the GA channel (Tian *et al* 1996, Tian and Cross 1999) find that the GA peptide remains rather rigid upon cation binding and the ion is solvated by just two carbonyl oxygens and two water molecules. Notwithstanding the difficulties

associated with inferring detailed structural information from solid-state NMR studies (cf. the discussion following Cross(1999)), one would normally expect such a serious discrepancy between theory and experiment to lead to a great deal of activity on both sides towards a quick resolution of the problem. Peculiarly, the experimental results have been mostly ignored by the MD community, despite their ramifications in modelling of GA and other channels with very narrow pore regions. The disagreement in ion coordination is significant because the missing solvation energy in the case of a rigid channel has to come from another source. One possible scenario is that the water molecules in the channel have, in fact, a more ordered structure than predicted by the current MD models of GA. Such an order could be induced by polarization interactions that would lower the energy of the ion–water column in the channel substantially.

Taken together, the above results identify a number of problems with the force fields currently used in MD simulations, and invite a consistent inclusion of polarization effects in future studies of GA. These problems are not unique for GA, but they could be easily identified in this case because the system allows for detailed comparison of the models with experiments. As would be expected, the appearance of the KcsA structure changed the focus of permeation models. In a way this is unfortunate because while the details of ion movement through GA channels are different from those formed by membrane proteins, the GA channels still remain the only system that allow for the necessary 'calibration' of the model calculations using experimental results. So, even though the incentive to pursue detailed studies on GA channels has become less, the amount of experimental results that is available for GA channels—which is much larger than for any other ion channel—means that they will retain their important role in the future development of ion permeation models. After all, it is difficult to know whether a model for the KcsA channel works simply because of the many 'free' parameters employed, or whether it reflects some deeper insights. That uncertainty is much less for GA channels, so models that have not been calibrated against GA channels will be less believable than those that have been.

4.2. KcsA potassium

The determination of the crystal structure of the KcsA potassium channel (Doyle *et al* 1998) is one of the most significant events in the history of ion channels that will have a lasting impact in the field (according to one measure, it has already been cited close to a thousand times). The revealed structure has ended decades of speculation by providing a vision for how biological ion channels could achieve a large conductance while maintaining their exquisite selectivity for particular ions. While KcsA is a bacterial potassium channel, quite different from those found in animals in many details (e.g. gating), two of its main features are expected to be preserved in all potassium channels: namely, the narrow selectivity filter with a 1.5 Å radius that holds two K^+ ions and a water-filled cavity that follows it (see the schematic above the plots in figure 4). The role of the filter is obvious and the cavity helps in reducing the self-energy barrier of ions (Roux and MacKinnon 1999). The significance of the KcsA structure actually transcends the potassium channels because it provides a general template for modelling all other biological channels. Not surprisingly, this has fired the imagination of many theorists from other fields and the interest in modelling of ion channels has been growing steadily. Below we review applications of the BD and MD methods to the KcsA channel (see also Sansom *et al* (2000)).

BD studies. The first BD study of KcsA was carried out using a simplified pore shape similar to a champagne glass and representing the charge residues on carbonyl groups in the selectivity filter and in the inner and outer mouths with dipoles (Chung *et al* 1999). This was followed by a

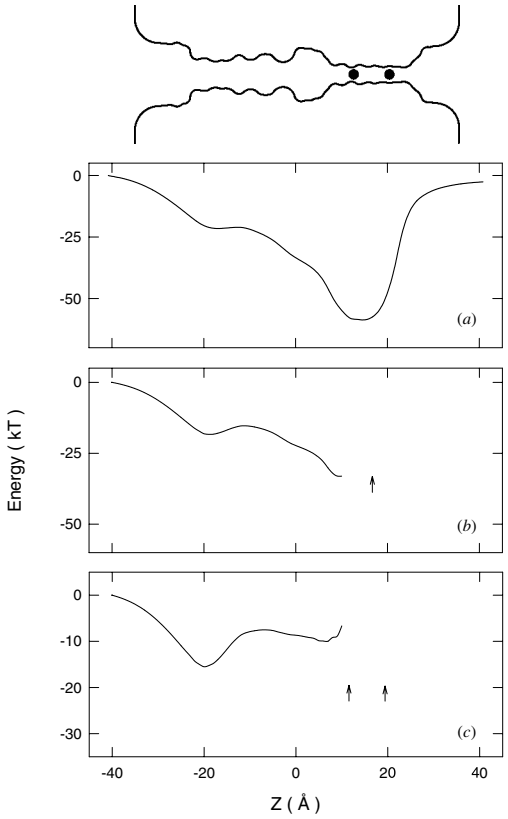

Figure 4. Potential energy profiles of a K^+ ion traversing the KcsA channel under an applied field of 10^7 V m^{-1} when there are 0 (*a*), 1 (*b*) and 2 (*c*) resident ions in the channel. The dielectric constants used in the solution of Poisson's equation are 60 for channel water and 2 for the protein. The electric field is in the z direction driving ions from inside the cell (left) to outside (right). The upward arrows indicate the location of the resident ions when the test ion is at the centre of the channel ($z = 0$ Å). The schematic above the plots shows the positions of the ions in case (*c*).

more sophisticated study that included all the experimentally determined channel protein in the model structure (Chung *et al* 2001). As the crystal structure of KcsA corresponds to its closed state, open-state configurations were constructed via MD simulations. The refinement has led to a better description of some properties (for example, positions of the K^+ ions in the channel were in better agreement with the experimentally observed sites) but otherwise corroborated the permeation mechanism found in the earlier study. We give an intuitive illustration of this mechanism using the multi-ion potential profiles obtained by minimizing the energies of ions resident in the channel while another ion is brought into the channel in small steps (figure 4). As seen in (*a*), there is a very deep well ($67kT$) for a single K^+ ion that will permanently bind it to the selectivity filter. The potential profile of a second ion (*b*) in the presence of the first one is again attractive though the well depth is reduced by about half. A third K^+ ion is still attracted to the channel from the intracellular side but now it faces a barrier of several kT high. Once it goes over this barrier through thermal fluctuations, it moves rapidly under the potential gradient towards the selectivity filter and destabilizes the equilibrium of the two resident ions there. From this point on, the three ions move more or less in tandem to the right until the right-most one is expelled from the channel, leaving again two K^+ ions in the filter.

This qualitative account of the permeation process in KcsA has been made quantitative by trajectory analysis of the BD simulations (Chung *et al* 1999, 2001). For example, the average concentration of ions in the channel, the average time an ion spends in various parts of the pore and its mean velocity provide complementary information about the ion dynamics. In the presence of a driving field, two ions are found in the filter and one near the inner mouth (see

figure 4(*c*)). Ions spend the most time in accessing the channel and climbing over the central barrier, the remaining time being negligible in comparison. As the first process depends on the concentration and the second does not, this provides a natural explanation for the saturation of current with increasing concentration. Similarly, analysis of the mean velocities shows that ions move at a fraction of their drift velocity in bulk while climbing the barrier but, once over, they move an order of magnitude faster. This explains the observed insensitivity of calculated current to diffusion coefficient of ions employed in BD simulations—a welcome result considering the uncertainties in the estimated values of diffusion coefficients from MD (see below).

The permeation mechanism delineated by the potential energy profiles and the BD simulations sheds much light on the central paradox in the operation of ion channels (i.e. large conductance versus selectivity), and how nature has solved this problem. The selectivity filter is very narrow to enable it to differentiate between potassium and sodium ions, and it has a very deep binding site. On the basis of these two factors, one would intuitively expect ions' crossing of the filter to be the rate-limiting step in the permeation process. In fact, Coulomb repulsion in the three-ion system causes it to be unstable, thereby making this the fastest step in permeation. A related puzzle concerns the large variations (nearly two orders of magnitude) observed in the conductance levels of various potassium channels. Clearly one could not explain such a diversity had the filter been the rate limiting step, because it is presumed to be conserved. Chung *et al* (2001) have found that the energy barrier in KcsA can be reduced substantially by increasing the radius of the inner mouth of the channel by a few ångstrom. Opening the mouth also makes the access of ions easier, thus increasing the current, but this alone is not sufficient to explain the observed variations. The more significant effect is the drop in the barrier height, which leads to an exponential growth in the current. Thus, the large conductance variations in potassium channels can be explained by changes in the radius of the intracellular mouth while keeping the selectivity filter on the opposite side intact.

The physiological properties of KcsA such as I–V and G–c curves have also been determined from the BD simulations (Chung *et al* 1999, 2001). Unfortunately, the available data in KcsA are too limited to allow detailed tests of the model calculations. Nevertheless, the calculated conductance G and half-saturation c_s values are found to be within the observed range (e.g. Cuello *et al* (1998), Meuser *et al* (1999), Heginbotham *et al* (1999)). We emphasize that use of the correct channel structure has been instrumental in obtaining results consistent with experiments in KcsA. The sensitivity of conductance to structural details has been demonstrated in recent BD simulations of an inward rectifier potassium channel (IRK1) that employed a theoretically developed structure—the calculated conductance was three orders of magnitude smaller than the experimental value (Hu *et al* 2000).

MD studies. Several groups have been involved in MD studies of KcsA (Guidoni *et al* 1999, 2000, Allen *et al* 1999b, 2000a, 2000b, Shrivastava and Sansom 2000, Biggin *et al* 2001, Ranatunga *et al* 2001, Åqvist and Luzhkov 2000, Luzhkov and Åqvist 2000, 2001, Bernèche and Roux 2000, Roux *et al* 2000). The main thrust of these studies has been to investigate permeation properties of KcsA such as ion binding sites, selectivity and diffusion, focusing especially on the filter region. An obvious reason for this is because that is where the K^+ ions have been observed. But also the crystal structure corresponds to the closed state, and our knowledge about the conformational changes that take place on the intracellular side during opening is still rudimentary (Perozo *et al* 1999). KcsA channels are opened by proton binding at the intracellular mouth, and channel opening is associated with a movement of the transmembrane helices near the mouth region. Another precaution about the x-ray structure is that it was determined at liquid nitrogen temperature (80 K), which may have induced subtle

rearrangements in crystal packing (Juers and Matthews 2001). Treatment of the lipid bilayer varied among the groups from using harmonic constraints (Allen *et al* 2000a, 2000b, Biggin *et al* 2001, Ranatunga *et al* 2001) to its explicit representation by octanes (Guidoni *et al* 1999, 2000), non-polar atoms (Luzhkov and Åqvist 2000, 2001) and phospholipids (Bernèche and Roux 2000, Shrivastava and Sansom 2000). Because explicit simulation of the lipid is quite time consuming, it would be worthwhile to seek an appropriate set of constraints that mimic the effects of embedding the KcsA protein in the lipid. As in the case of GA, nonpolarizable force fields are employed in all MD simulations of KcsA so far. Therefore, the absolute values of the calculated free energies has to be interpreted with caution.

There is a general agreement among the MD simulations that the KcsA protein can hold three K^+ ions in a stable conformation, two in the filter and one in the central cavity, as observed in the x-ray structure (Doyle *et al* 1998). There have been only a few calculations of free-energy profiles so far (Allen *et al* 1999b, 2000b) that find no significant barriers for a K^+ ion in the channel. Of course, unlike GA, KcsA is a multi-ion channel and not much can be surmised from the single-ion profiles (see the changes in electrostatic energies in figure 4 as the channel is loaded with ions). Calculation and interpretation of the multi-ion free-energy profiles in KcsA remains as a future challenge. Ion selectivity of KcsA is of primary interest for MD simulations both because of its biological significance and also because of the inability of the BD method to differentiate between monovalent cations. Free-energy perturbation calculations for the transformation $K^+ \rightarrow Na^+$ predict relative barriers of $\sim 8kT$ for sodium permeation, (Allen *et al* 2000b, Åqvist and Luzhkov 2000), sufficient to explain the observed selectivity ratio of 10^4. As stressed earlier, free energy differences are less sensitive to model details, making these results more robust. Further study of coordination of potassium and sodium ions in the filter shows that the carbonyl oxygens provide a bulk-like solvation environment for K^+ but fail to do so for Na^+ (Allen *et al* 1999b, 2000b, Biggin *et al* 2001). According to the picture emerging from these studies, the filter is quite rigid and its size is optimized for solvation of the K^+ ions (radius 1.33 Å). Therefore, the smaller Na^+ ions with radius 0.95 Å are not as well hydrated and are rejected from the channel. This 'rigid filter' picture has been contested by more detailed simulations of KcsA in a lipid bilayer (Shrivastava and Sansom 2000, Bernèche and Roux 2000), which found sizeable RMS fluctuations ($\sim$1 Å) of the residues forming the filter. On this basis, it was concluded that selectivity must have a more complicated origin, arising from subtle ion–water–protein interactions. Unfortunately, this conjecture was not backed up by any hard numbers but justified by appealing to the flexibility of the GA peptide as observed in MD simulations. As mentioned earlier, solid-state NMR experiments indicate a rather rigid structure for the GA channel structure. It will be very important to clarify this rigid versus flexible filter issue by repeating the NMR experiments for the KcsA channel.

Diffusion of ions and water in KcsA have been studied by Allen *et al* (1999b, 2000a, 2000b) and Biggin *et al* (2001). Author: Please check Allen et al 1999a or 1999b?The main finding from these studies is that the diffusion coefficient of K^+ ions is suppressed down to about 10% of the bulk value in the filter region but remains relatively high (>50% of bulk value) in the rest of the channel. As mentioned in the discussion of BD results, permeation dynamics in the filter region is dominated by Coulomb repulsion during a conduction event, and despite the large suppression of the diffusion coefficient, this is actually the fastest step in permeation. Motion of individual ions in the channel have also been discussed in MD studies of KcsA. However, such single-event studies have little meaning statistically, and cannot be used to draw conclusions about permeation dynamics.

An important issue that we have not touched upon is the charge states of ionizable residues in the KcsA protein. The BD simulations show that charges on some of these residues can have a dramatic effect on the channel conductance (Chung *et al* 2001). Unfortunately, the

protonation states in KcsA are calculated using the PB theory (Roux *et al* 2000, Ranatunga *et al* 2001), and in view of its demonstrated breakdown in narrow pores, such calculations are not reliable. Until this problem is resolved satisfactorily there will be continuing doubts about the authenticity of the calculated energies.

The appearance of the KcsA structure has also instigated MD studies of other potassium channels through homology modelling (Capener *et al* 2000, Shrivastava *et al* 2000). These first exploratory studies are expected to be followed up by more sophisticated ones that tackle the gating mechanism in voltage- and ligand-gated potassium channels, one of the current frontiers in ion channel studies.

4.3. L-type calcium

Calcium channels are as ubiquitous in excitable cells as potassium channels and share similar properties, that is, they are extremely selective (the margin for Ca/Na is 10^3) and yet conduct at the picoampere level (Tsien *et al* 1987). But there is also a crucial difference: selectivity is based on charge and not size. The radius of the Ca^{2+} ion (0.99 Å) is only slightly larger than that of Na^+ while the pore radius is estimated to be about 2.8 Å (McCleskey and Almers 1985). Thus, selectivity of calcium channels can be understood at the BD level without having to appeal to MD. An intriguing feature of this selectivity against Na^+ ions is that it is contingent upon the presence of Ca^{2+} ions. In their absence, Na^+ ions conduct at an even faster rate than Ca^{2+}. The physiological properties of calcium channels are well known but the corresponding information on the structural side is rather scarce, i.e. their tertiary structures have not been determined from crystallography yet. This puts a dampener on attempts to model calcium channels using MD simulations because they are quite sensitive to structural details, and it would be very difficult to get sensible results out of MD in such circumstances. Fortunately, structural requirements for BD simulations are much less demanding—an approximate shape of the channel and positions of the partial charges in the protein are all one needs to model its functional properties. Such an attempt has recently been made by Corry *et al* (2000b, 2001), who carried out BD simulations of a model L-type calcium channel. Their results are very encouraging, giving hope that properties of many other channels without a known tertiary structure could be studied using the BD method. For this reason, we include a brief account of this BD study here.

The shape of the calcium channel used in the model study is shown in the inset of figure 5. It is inspired by the KcsA structure but modified to take into account the available structural and physiological data on the L-type calcium channel. Four glutamate residues are known to play an essential role in the channel conductivity and selectivity (Yang *et al* 1993), and these are represented by four negative charges in the narrow selectivity filter (indicated by squares in the figure). The only other charge residues required to make the channel conduct are the set of four dipoles placed on the intracellular mouth (diamonds in the figure). As in the KcsA study, multi-ion potential profiles give an intuitive understanding of the permeation mechanism in the calcium channel. As shown in figure 5(*a*), a single Ca^{2+} ion would be strongly bound (binding energy $58kT$) in the selectivity filter. A second Ca^{2+} ion is attracted to the channel from the extracellular (right) side, and the two ions can coexist in the filter region in a semi-stable equilibrium, until the resident ion on the left climbs over the barrier of $5kT$ via thermal fluctuations and exits the channel. A similar picture is obtained for the Na^+ ions (*b*), except that three of them can coexist in the filter and the final barrier to permeation is only $1kT$, which explains why the sodium ions conduct faster. Selectivity of the calcium channel can be understood by constructing multi-ion profiles with a mixed set of ions (figure 5(*c*)). When a Na^+ ion is resident in the filter, a Ca^{2+} ion is attracted to the filter and expels the Na^+ ion from

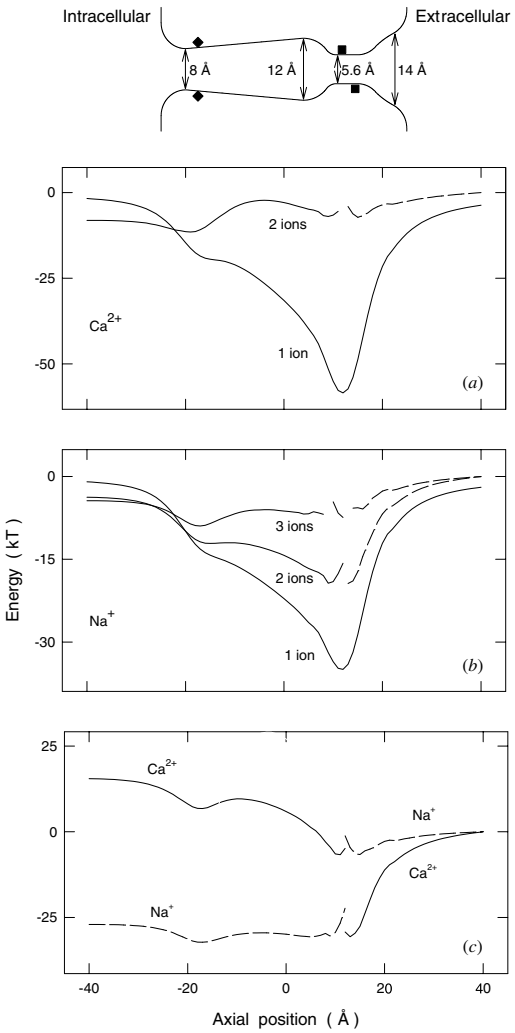

Figure 5. Shape of a model calcium channel and locations of charge residues (inset). Potential energy profiles for one and two Ca^{2+} ions (*a*), and one, two and three Na^{+} ions (*b*). The profiles for the mixed system is shown in (*c*). The parameters are as in figure 4 except that the electric field is reversed to the inward direction (right to left).

the channel upon entry. A similar result is obtained when there are two Na^{+} ions in the filter. In the reverse case of a Ca^{2+} ion in the filter, though a Na^{+} ion is still attracted, it is unable to push the Ca^{2+} ion over the large barrier of $16kT$. Thus once a Ca^{2+} ion enters the channel, Na^{+} ions cannot push it out, only another Ca^{2+} ion can achieve that feat. This gives a simple explanation of the selectivity mechanism in calcium channels in terms of the electrostatic interactions of ions, which is in conformity with the insights gathered from the rate theory models (McCleskey 1999). Though not to the same degree as above, calcium channels also exhibit selectivity among ions with the same valence. Explanation of this property, however, requires MD simulations and has to wait for more structural information.

A number of physiological properties of calcium channels have been determined from the BD simulations (Corry *et al* 2001). For example, the I–V and G–c curves are found to be in good agreement with the experimental observations. We will not dwell on these standard quantities here but rather discuss a few other exotic properties of calcium channels that have been elucidated by these calculations. The first is the anomalous mole fraction effect, so called because the channel current vanishes at a certain range of Ca^{2+} concentrations

in the presence of a fixed 0.15 M Na^+, as shown in the inset of figure 6(*a*). The BD results indicate that the rapid drop and subsequent vanishing of the channel current is due to the blocking of Na^+ current by Ca^{2+} ions. Once the Ca^{2+} concentration is high enough to allow two Ca^{2+} ions in the filter, the channel starts conducting again, but now Ca^{2+} ions instead of Na^+. While sodium ions cannot block calcium, their presence in the vestibule can nevertheless slow down entry of a second Ca^{2+} ion necessary for conduction. As illustrated in figure 6(*b*), the predicted reduction in the channel current with increasing Na^+ concentration is in excellent agreement with the experimental data. A final example is the effect of mutating one of the glutamate residues to neutral glutamine on the blocking of Na^+ current (figure 6(*c*)). The mutation leads to a reduction in the depth of the potential well compared with the native case so that entry of a Ca^{2+} ion in the channel is delayed, and the blocking occurs at a higher Ca^{2+} concentration. Trends in the data (inset of (*c*)) are again reproduced by the BD simulations.

5. Conclusions

The main conclusions of this review can be summarized as follows:

- Self-energy is an important part of an ion's potential energy in channels, responsible for many properties through creation of energy barriers. This contribution is ignored in current continuum theories, and therefore they cannot describe the physics of narrow pores with radii 2–5 Å correctly. We recommend that, until this self-energy problem is satisfactorily resolved, continuum theories should not be used in modelling of ion channels.
- At present, the BD and MD methods that treat ions as discrete particles provide the best alternatives for studying the structure–function relations in ion channels. The former enables calculation of conductance properties while the latter can provide input for BD as well as explaining finer details such as size-based selectivity. As practiced, both methods have unjustified approximations and deficiencies that need to be better understood and improved in future work. For example, use of continuum electrostatics in calculation of forces in BD simulations needs to be better validated by appealing to MD. Similarly, the force fields employed in MD simulations should be improved by including polarization effects. *Ab initio* MD would provide a useful guide in this endeavour.
- These improvements in force fields will need to be calibrated against experimental results, where the GA channels remain a system of choice. Partly because of the large amount of experimental information that is available, and partly because GA simulations have proven to be a demanding test bench—any modelling approach that passes the GA test is likely to have wide applicability.
- Studies of potassium and calcium channels using continuum electrostatics and BD demonstrate that the permeation mechanism involves multi-ions, and Coulomb repulsion among the ions plays an essential role in explaining the central paradox of ion channels: that is, the fast permeation of ions across a binding site (i.e. the selectivity filter). Comparisons of the BD simulation results with the experimental observations are very encouraging for future applications of this method as they indicate that basic properties of ion channels can be understood using a simplified model in the absence of a detailed tertiary structure. This has far-reaching implication for modelling of ion channels because MD simulations require a detailed knowledge of the channel structure whereas only a few channels have been resolved from crystallography so far. Thus BD offers the only practical method for studying the structure–function relationships in biological ion channels at present, and one would like to see more modelling efforts expended in this direction.

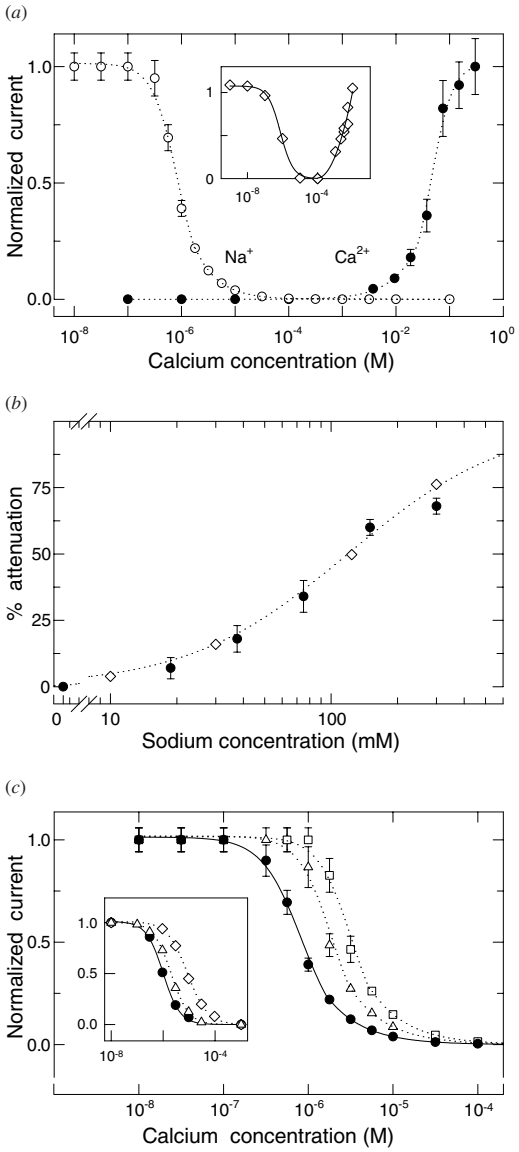

Figure 6. (*a*) Mole fraction effect. Ca^{2+} (filled circles) and Na^{+} (open circles) current passing through the channel normalized by the maximum value of each is plotted against the Ca^{2+} concentrations while keeping the Na^{+} concentration fixed at 0.15 M. Experimental results from Almers *et al* (1984) are shown in the inset. (*b*) Attenuation of Ca^{2+} current by Na^{+} ions. The percentage reduction in the channel current is plotted against Na^{+} concentration while the Ca^{2+} concentration is fixed at 0.15 M (filled circles). The open diamonds and dotted curve show the experimental data from Polo-Parada and Korn (1997). (*c*) The effect of removing glutamate charges on channel selectivity: the Na^{+} current passing through the channel at different Ca^{2+} concentrations with all four glutamate charges in place (filled circles), the outermost glutamate removed (triangles) and the innermost glutamate removed (squares); otherwise all conditions are as in (*a*). Experimental data for wild type (filled circles) and for single glutamate to neutral glutamine mutations of two different residues (triangles and diamonds) are shown in the inset (Yang *et al* 1993). In all cases a driving potential of −0.2 V is applied.

We hope that this review will induce readers from other fields to join in the exciting research into ion channels and contribute to the applications and refinement of the permeation models currently used in their description.

Acknowledgments

This work is supported in part by grants from the Australian Research Council and the National Health and Medical Research Council of Australia and the National Institutes of Health of USA. We thank our collaborators Toby Allen, Ben Corry, Scott Edwards, Matthew Hoyles and Siu-Cheung Li, who have contributed to the BD and MD studies of channels reported in this review.

Author: Any more details to be included in Chung et al (2000), Corry et al (2001b), Edwards et al (2001) and Tieleman et al (2001)?

References

Adcock C, Smith G R and Sansom M S P 1998 *Biophys. J.* **75** 1211–22
——2000 *Eur. Biophys. J.* **29** 29–37
Allen T W, Kuyucak S and Chung S H 1999a *J. Chem. Phys.* **111** 7985–99
——1999b *Biophys. J.* **77** 2502–16
——2000a *Biophys. Chem.* **86** 1–14
Allen T W, Bliznyuk A, Rendell A P, Kuyucak S and Chung S H 2000b *J. Chem. Phys.* **112** 8191–204
Allen M P and Tildesley D J 1987 *Computer Simulation of Liquids* (London: Oxford University Press)
Almers W, McCleskey E W and Palade P T 1984 *J. Physiol.* **353** 565–83
Andersen O S 1978 Permeability properties of unmodified lipid bilayer membranes. *Membrane Transport in Biology*, Eds. Giebisch G, Tosteson D C and Ussing HH (New York: Springer) bf 1 369–446
Andersen O S 1983 *Biophys. J.* **41** 147–65
Andersen O S 1989a *Ann. N. Y. Acad. Sci.* **574** 333–53
Andersen O S 1989a *Meth. Enzymol.* **171** 62–112
Andersen O S and Procopio J 1980 *Acta. Physiol. Scand.; Suppl.* **481** 27–35
Andersen O S and Koeppe R E 1992 *Physiol. Rev.* **72** 89–158
Åqvist J and Luzhkov V 2000 *Nature* **404** 881–4
Arseniev A S, Barsukov I L, Bystrov V F and Ovchinnikov Yu A 1986 *Biol. Membr.* **3** 437–62
Barnes P, Finney J L, Nichols J D and Quinn J E 1979 *Nature* **282** 459–64
Batista E R, Xantheas S S and Jonsson H 1998 *J. Chem. Phys.* **109** 4546–51
Bean R C, Shepperd W C, Chna M and Eichner J 1969 *J. Gen. Physiol.* **53** 741–57
Becker M D, Koeppe R E and Andersen O S 1992 *Biophys. J.* **62** 25–7
Bek S and Jakobsson E 1994 *Biophys. J.* **66** 1028–38
Berendsen H J C, Grigera J R and Straatsma T P 1987 *J. Phys. Chem.* **91** 6269–71
Berendsen H J C, Postma J P M, van Gunsteren W F and Hermans J 1981 *Intermolecular Forces* ed B Pullman (Dordrecht: Reidel) pp 331–42
Bernèche S and Roux B 2000 *Biophys. J.* **78** 2900–17
Bezanilla F 2000 *Phys. Rev.* **80** 555–92
Bickelhaupt F M and Baerends E J 2000 *Rev. Comput. Chem.* **15** 1–86
Biggin P C, Smith G R, Shrivastava I, Choe S and Sansom M S P 2001 *Biochim. Biophys. Acta.* **1510** 1–9
Bockris J O' M and Reddy A K N 1970 *Modern Electrochemistry* (New York: Plenum)
Brooks B R, Bruccoleri R E, Olafson B D, States D J, Swaminathan S and Karplus M 1983 *J. Comput. Chem.* **4** 187–217
Busath D D 1993 *Ann. Rev. Physiol.* **55** 473–501
Cai M and Jordan P C 1990 *Biophys. J.* **57** 883–91
Capener C E, Shrivastava I H, Ranatunga K M, Forrest L C, Smith G R and Sansom M S P 2000 *Biophys. J.* **78** 2929–42
Car R and Parrinello M 1985 *Phys. Rev. Lett.* **55** 2471–4
Cardenas A E, Coalson R D and Kurnikova M G 2000 *Biophys. J.* **79** 80–93
Chandrasekhar S 1943 *Rev. Mod. Phys.* **15** 1–89
Chang G, Spencer R H, Lee A T, Barclay M T and Rees D C 1998 *Science* **282** 2220–6
Cheng W, Wang C X, Chen W Z, Xu Y W and Shi Y Y 1998 *Eur. Biophys. J.* **27** 105–12
Chiu S W, Subramaniam S and Jakobsson E 1999 *Biophys. J.* **76** 1929–50
Chung S H, Allen T W, Hoyles M and Kuyucak S 1999 *Biophys. J.* **77** 2517–33
Chung S H, Allen T W and Kuyucak S 2001 *Biophys. J.* at press
Chung S H, Hoyles M, Allen T W and Kuyucak S 1998 *Biophys. J.* **75** 793–809
Chung S H and Kuyucak S 1995 *Neurosci. Lett.* **187** 181–4
Clough S A, Beers Y, Klein G P and Rothman L S 1973 *J. Chem. Phys.* **59** 2254–9
Cooper K E, Gates P Y and Eisenberg R S 1988 *Q. Rev. Biophys.* **21** 331–64
Cooper K E, Jakobsson E and Wolynes P 1985 *Prog. Biophys. Mol. Biol.* **46** 51–96
Corry B, Hoyles M, Allen T W, Walker M, Kuyucak S and Chung S H 2001b *Biophys. J.* submitted
Corry B, Kuyucak S and Chung S H 2000a *Biophys. J.* **78** 2364–81
Corry B, Allen T W, Kuyucak S and Chung S H 2000b *Biochim. Biophys. Acta* **1509** 1–6

——2001 *Biophys. J.* **80** 195–214
Coulson C A and Eisenberg D 1966 *Proc. R. Soc.* A **291** 445–53
Cross T A, Tian F, Cotton M, Wang J, Kovacs F and Fu R 1999 In *Gramicidin and related ion channel – forming peptides.* Novartis Foundation Symposium **225** 4–22
Crozier P S, Rowley R L, Holladay N B, Henderson D and Busath D D 2001 *Phys. Rev. Lett.* **86** 2467–70
Cuello L G, Romero J G, Cortes D M and Perozo E 1998 *Biochemistry* **37** 3229–36
Dang L X 1992 *J. Chem. Phys.* **97** 2659–60
Dang L X and Chang T M 1997 *J. Chem. Phys.* **106** 8149–59
Davis M E and McCammon J A 1990 *Chem. Rev.* **90** 509–21
Dieckmann G R, Lear J D, Zhong Q, Klein M L, DeGrado W F and Sharp K A 1999 *Biophys. J.* **76** 618–30
Dorman V, Partenskii M B and Jordan P C 1996 *Biophys. J.* **70** 121–34
Doyle D A, Cabral J M, Pfuetzner R A, Kuo A, Gulbis J M, Cohen S L, Chait B T and MacKinnon R 1998 *Science* **280** 69–77
Dreizler R M and Gross E K U 1991 *Density Functional Theory* (Berlin: Springer)
Duca K A and Jordan P C 1997 *Biophys. Chem.* **65** 123–41
——1998 *J. Phys. Chem.* **102** 9127–38
Edwards S, Corry B, Kuyucak S and Chung S H 2001 *Biophys. J.* submitted
Eisenberg R S 1996 *J. Membr. Biol.* **150** 1–25
——1999 *J. Membr. Biol.* **171** 1–24
Eisenman G and Horn R 1983 *J. Membrane Biol.* **76** 197–225
Engkvist O, Åstrand P O and Karlström G 2000 *Chem. Rev.* **100** 4087–108
Frenkel D and Smit B 1996 *Understanding Molecular Simulation: From Algorithms to Applications* (San Diego: Academic)
Geissler P L, Dellago C, Chandler D, Hutter J and Parrinello M 2001 *Science* **291** 2121–4
Green M E and Lu J 1997 *J. Phys. Chem.* B **101** 6512–24
Guàrdia E, Rey R and Padró J A 1991a *Chem. Phys.* **155** 187–95
——1991b *J. Chem. Phys.* **95** 2823–31
Guidoni L, Torre V and Carloni P 1999 *Biochemistry* **38** 8599–604
——2000 *FEBS Lett.* **477** 37–42
Guillot B and Guissani Y 2001 *J. Chem. Phys.* **114** 6720–33
Halgren T A and Damm W 2001 *Curr. Opin. Sruct. Biol.* **11** 236–42
Hamill O P, Marty A, Neher E, Sakmann B and Sigworth F J 1981 *Pflügers Arch.* **391** 85–100
Heginbotham L, LeMasurier M, Kolmakova-Partensky L and Miller C 1999 *J. Gen. Physiol.* **114** 551–9
Hellemans A 1999 *Science* **283** 614
Hermans J, Berendsen H J C, van Gunsteren W F and Postma J P M 1984 *Biopolymers* **23** 1513–8
Hille B 1992 *Ionic Channels of Excitable Membranes* 2nd edn (Sunderland, MA: Sinauer Associates)
Hladsky S B and Haydon D A 1970 *Nature* **225** 451–3
Höchtl P, Boresch S, Bitomsky W and Steinhauser O 1998 *J. Chem. Phys.* **109** 4927–37
Hollerbach U, Chen D P, Busath D D and Eisenberg B 2000 *Langmuir* **16** 5509–14
Honig B and Nicholls A 1995 *Science* **268** 1144–9
Hoyles M, Kuyucak S and Chung S H 1996 *Biophys. J.* **70** 1628–42
——1998a *Phys. Rev.* E **58** 3654–61
——1998b *Comput. Phys. Commun.* **115** 45–68
Hu J, Goodman S, Gray C G and Guy H R 2000 *Mol. Phys.* **98** 535–47
Im W, Seefeld S and Roux B 2000 *Biophys. J.* **79** 788–801
Isaacs E D, Shukla A, Platzman P M, Hamann D R, Barbiellini B and Tulk C A 1999 *Phys. Rev. Lett.* **82** 600–3
Jackson M B 1989 *Proc. Natl. Acad. Sci. USA* **86** 2199–203
Jakobsson E and Chiu S W 1987 *Biophys. J.* **52** 33–45
Jordan P C 1982 *Biophys. J.* **39** 157–64
——1984 *Biophys. J.* **45** 1091–100
——1987 *J. Phys. Chem.* **91** 6582–91
——1990 *Biophys. J.* **58** 1133–56
Jordan P C, Bacquet R J, McCammon J A and Tran P 1989 *Biophys. J.* **55** 1041–52
Jorgensen W L, Chandrasekhar J, Madura J D, Impey R W and Klein M L 1983 *J. Chem. Phys.* **79** 926–35
Juers D H and Matthews B W 2001 *J. Mol. Biol.* **311** 851–62
Ketchem R R, Roux B and Cross T A 1997 *Structure* **5** 1655–69
Koeppe R E and Andersen O S 1996 *Ann. Rev. Biophys. Biomol. Struct.* **25** 231–58
Kohn W 1999 *Rev. Mod. Phys.* **71** 1253–66

Kohn W, Becke A D and Parr R G 1996 *J. Phys. Chem.* **100** 12974–80
Koneshan S, Rasaiah J C and Dang L X 2001 *J. Chem. Phys.* **114** 7544–55
Kubo R 1966 *Rep. Prog. Phys.* **29** 255–84
Kurnikova M G, Coalson R D, Graf P and Nitzan A 1999 *Biophys. J.* **76** 642–56
Kuyucak S and Chung S H 1994 *Biophys. Chem.* **52** 15–24
Kuyucak S, Hoyles M and Chung S H 1998 *Biophys. J.* **74** 22–36
Laasonen K, Sprik M, Parrinello M and Car R 1993 *J. Chem. Phys.* **99** 9080–9
Lee W K and Jordan P C 1984 *Biophys. J.* **46** 805–19
Lehmann-Horn F and Jurkatt-Rott K 1999 *Physiol. Rev.* **79** 1317–72
Levitt D G 1978 *Biophys. J.* **22** 209–19
——1985 *Biophys. J.* **48** 19–31
——1986 *Ann. Rev. Biophys. Biophys. Chem.* **15** 29–57
——1999 *J. Gen. Physiol.* **113** 789–94
Li S C, Hoyles M, Kuyucak S and Chung S H 1998 *Biophys. J.* **74** 37–47
Luzhkov V B and Åqvist J 2000 *Biochim. Biophys. Acta* **1481** 360–70
——2001 *FEBS Lett.* **495** 191–6
Lyubartsev A P, Laasonen K and Laaksonen A 2001 *J. Chem. Phys.* **114** 3120–6
Madura J D, Briggs J M, Wade R C, Davis M E, Brock A, Ilin A, Antosiewicz J, Gilson M K, Bagheri B, Scott L R and McCammon A 1995 *Comput. Phys. Commun.* **91** 57–95
Martin T W and Derewenda Z S 1999 *Nature Struct. Biol.* **6** 403–6
Marx D, Sprik M and Parrinello M 1997 *Chem. Phys. Lett.* **273** 360–6
Matsuoka O, Clementi E and Yoshimine M 1976 *J. Chem. Phys.* **64** 1351–61
McCleskey E W 1999 *J. Gen. Physiol.* **113** 765–72
McCleskey E W and Almers W 1985 *Proc. Natl Acad. Sci. USA* **82** 7149–53
McQuarrie D A 1976 *Statistical Mechanics* (New York: Harper Collins)
Meuser D, Splitt H, Wagner R and Schrempf H 1999 *FEBS Lett.* **462** 447–52
Miller C 1999 *J. Gen. Physiol.* **113** 783–7
Monoi H 1991 *Biophys. J.* **59** 786–94
Moy G, Corry B, Kuyucak S and Chung S H 2000 *Biophys. J.* **78** 2349–63
Neher E and Sakmann B 1976 *Nature* **260** 799–802
Neher E, Sandblom J and Eisenman G 1978 *J. Membrane Biol* **40** 97–116
Nonner W, Catacuzzeno L and Eisenberg B 2000 *Biophys. J.* **79** 1976–92
Nonner W, Chen D and Eisenberg B 1998 *Biophys. J.* **74** 2327–34
——1999 *J. Gen. Physiol.* **113** 773–82
Nonner W and Eisenberg B 1998 *Biophys. J.* **75** 1287–305
Parr R G and Yang W 1989 *Density Functional Theory of Atoms and Molecules* (Oxford: Oxford University Press)
Parrinello M 1997 *Solid State Commun.* **102** 107–20
Parsegian A 1969 *Nature* **221** 844–6
Partenskii M B, Dorman V and Jordan P C 1994 *Biophys. J.* **67** 1429–38
Partenskii M B and Jordan P C 1992 *Q. Rev. Biophys.* **25** 477–510
Perozo E, Cortes D M and Cuello L G 1999 *Science* **285** 73–8
Polo-Parada L and Korn S J 1997 *J. Gen. Physiol.* **109** 693–702
Pople J A 1999 *Rev. Mod. Phys.* **71** 1267–74
Probst M M, Spohr E and Heinzinger K 1989 *Chem. Phys. Lett.* **161** 405–8
Pullman A 1987 *Q. Rev. Biophys.* **20** 173–200
Ramaniah L M, Bernasconi M and Parrinello M 1999 *J. Chem. Phys.* **111** 1587–91
Ranatunga K M, Adcock C, Kerr I D, Smith G R and Sansom M S P 1999 *Theor. Chem. Acc.* **101** 97–102
Ranatunga K M, Shrivastava I H, Smith G R and Sansom M S P 2001 *Biophys. J.* **80** 1210–9
Rapaport D C 1995 *The Art of Molecular Dynamics Simulation* (Cambridge: Cambridge University Press)
Rey R, Guàrdia E and Padró J A 1992 *J. Chem. Phys.* **97** 1343–52
Rick S W, Stuart S J and Berne B J 1994 *J. Chem. Phys.* **101** 6141–56
Romero A H, Silvestrelli P G and Parrinello M 2001 *J. Chem. Phys.* **115** 115–23
Rostovtseva T K, Aguilella V M, Vodyanoy I, Bezrukov S M and Parsegian V A 1998 *Biophys. J.* **75** 1783–92
Roux B 1996 *Biophys. J.* **71** 3177–85
Roux B and Karplus M 1993 *J. Am. Chem. Soc.* **115** 3250–62
——1994 *Ann. Rev. Biophys. Biomol. Struct.* **23** 731–61
Roux B, Berneche S and Im W 2000 *Biochemistry* **39** 13295–306
Roux B and MacKinnon R 1999 *Science* **285** 100–2

Roux B, Prodhom B and Karplus M 1995 *Biophys. J.* **68** 876–92
Rullmann J A C and van Duijnen P T 1988 *Mol. Phys.* **63** 451–75
Sagnella D E, Laasonen K and Klein M L 1996 *Biophys. J.* **71** 1172–8
Sancho M, Partenskii M B, Dorman V and Jordan P C 1995 *Biophys. J.* **68** 427–33
Sankararamakrishnan R, Adcock C and Sansom M S P 1996 *Biophys. J.* **71** 1659–71
Sansom M S P, Adcock C and Smith G R 1998 *J. Struct. Biol.* **121** 246–62
Sansom M S P, Kerr I D, Breed J and Sankararamakrishnan R 1996 *Biophys J.* **70** 693–702
Sansom M S P, Smith G R, Adcock C and Biggin P C 1997 *Biophys. J.* **73** 2404–15
Sansom M S P, Shrivastava I H, Ranatunga K M and Smith G R 2000 *Trends Biochem. Sci.* **25** 368–74
Schirmer T and Phale P S 1999 *J. Mol. Biol.* **294** 1159–67
Sharp K A and Honig B 1990 *Ann. Rev. Biophys. Biophys. Chem.* **19** 301–32
Shrivastava I H, Capener C E, Forrest L R and Sansom M S P 2000 *Biophys. J.* **78** 79–92
Shrivastava I H and Sansom M S P 2000 *Biophys. J.* **78** 557–70
Silvestrelli P L and Parrinello M 1999 *J. Chem. Phys.* **111** 3572–80
Sprik M 1991 *J. Chem. Phys.* **95** 6762–9
Sprik M, Hutter J and Parrinello M 1996 *J. Chem. Phys.* **105** 1142–52
Sprik M and Klein M L 1988 *J. Chem. Phys.* **89** 7556–60
Suenaga A, Komeiji Y, Uebayasi M, Meguro T, Saito M and Yamato I 1998 *Biosci. Rep.* **18** 39–48
Syganow A and von Kitzing E 1999a *Biophys. J.* **76** 768–81
——1999b *Eur. Biophys. J.* **28** 393–414
Tian F and Cross T A 1999 *J. Mol. Biol.* **285** 1993–2003
Tian F, Lee K C, Hu W and Cross T A 1996 *Biochemistry* **35** 11959–66
Tieleman D P, Marrink S J and Berendsen H J C 1997 *Biochim. Biophys. Acta.* **1331** 235–70
Tieleman D P and Berendsen H J C 1998 *Biophys. J.* **74** 2786–801
Tieleman D P, Biggin P C, Smith G R and Sansom M S P 2001 *Q. Rev. Biophys.* at press
Tobias D J, Jungwirth P and Parrinello M 2001 *J. Chem. Phys.* **114** 7036–44
Townsley L E, Tucker A W, Sham S and Hinton J F 2001 *Biochemistry* **40** 11676–86
Toyoshima C and Unwin N 1988 *Nature* **336** 247–50
Tsien R W, Hess P, McCleskey E W and Rosenberg R L 1987 *Ann. Rev. Biophys. Chem.* **16** 265–90
Tuckerman M E and Martyna G J 1999 *J. Phys. Chem.* B **104** 159–78
Tuckerman M E, Ungar P J, von Rosenvinge T and Klein M L 1996 *J. Phys. Chem.* **100** 12878–87
Unwin P N T and Ennis P D 1984 *Nature* **307** 609–13
Unwin N 1995 *Nature* **373** 37–43
Urban B W, Hladky S B and Haydon D A 1980 *Biochim. Biophys. Acta* **602** 331–54
Urry D W 1971 *Proc. Natl Acad. Sci. USA* **68** 672–6
van Gunsteren W F and Berendsen H J C 1982 *Mol. Phys.* **45** 637–47
Verlet L 1967 *Phys. Rev.* **159** 98–103
Wallace B A 1998 *J. Struct. Biol.* **121** 123–41
Wallqvist A and Karlström G 1989 *Chem. Scr.* A **29** 131
Wallqvist A and Mountain R D 1999 *Rev. Comput. Chem.* **13** 183–247
Warshel A and Åqvist J 1991 *Ann. Rev. Biophys. Biophys. Chem.* **20** 267–98
Weetman P, Goldman S and Gray C G 1997 *J. Phys. Chem.* **101** 6073–8
Weiner S J, Kollman P A, Case D A, Singh U C, Ghio C, Alagona G, Profeta S and Weiner P 1984 *J. Am. Chem. Soc.* **106** 765–84
Weiss M S, Kreusch A, Schlitz E, Nestel U, Welte W, Weckesser J and Schultz G E 1991 *FEBS Lett.* **280** 379–82
White J D, Schwegler E, Galli G and Gygi F 2000 *J. Chem. Phys.* **113** 4668–73
Woolf T B and Roux B 1994 *Proc. Natl Acad. Sci. USA* **91** 11631–5
——1997 *Biophys. J.* **72** 1930–45
Yang J, Ellinor P T, Sather W A, Zhang J F and Tsien R W 1993 *Nature* **366** 158–61
Zhang L, Davis H T, Kroll D M and White H S 1995 *J. Phys. Chem.* **99** 2878–84